Sequence-Specific Protein Aggregation Generates Defined Protein Knockdowns in Plants[1][OPEN]

Camilla Betti, Isabelle Vanhoutte, Silvie Coutuer[2], Riet De Rycke, Kiril Mishev[3], Marnik Vuylsteke, Stijn Aesaert, Debbie Rombaut, Rodrigo Gallardo, Frederik De Smet[4], Jie Xu[5], Mieke Van Lijsebettens, Frank Van Breusegem, Dirk Inzé, Frederic Rousseau*, Joost Schymkowitz*, and Eugenia Russinova*

Department of Plant Systems Biology, VIB, 9052 Gent, Belgium (C.B., I.V., S.C., R.D.R., K.M., S.A., D.R., M.V.L., F.V.B., D.I., E.R.); Department of Plant Biotechnology and Bioinformatics, Ghent University, 9052 Gent, Belgium (C.B., I.V., S.C., R.D.R., K.M., S.A., D.R., M.V.L., F.V.B., D.I., E.R.); Switch Laboratory, VIB, 3000 Leuven, Belgium (R.G., F.D.S., J.X., F.R., J.S.); Switch Laboratory, Department of Cellular and Molecular Medicine, University of Leuven, 3000 Leuven, Belgium (R.G., F.D.S., J.X., F.R., J.S); and Gnomixx, 9000 Gent, Belgium (M.V.)

ORCID IDs: 0000-0003-3522-6440 (C.B.); 0000-0003-2878-134X (I.V.); 0000-0002-7539-1005 (S.C.); 0000-0001-8270-7015 (R.D.R.); 0000-0001-5849-8786 (K.M.); 0000-0003-1584-3564 (R.G.); 0000-0002-3147-0860 (F.V.B.); 0000-0002-3217-8407 (D.I.); 0000-0003-2020-0168 (J.S.); 0000-0002-0569-1977 (E.R.).

Protein aggregation is determined by short (5–15 amino acids) aggregation-prone regions (APRs) of the polypeptide sequence that self-associate in a specific manner to form β-structured inclusions. Here, we demonstrate that the sequence specificity of APRs can be exploited to selectively knock down proteins with different localization and function in plants. Synthetic aggregation-prone peptides derived from the APRs of either the negative regulators of the brassinosteroid (BR) signaling, the glycogen synthase kinase 3/Arabidopsis SHAGGY-like kinases (GSK3/ASKs), or the starch-degrading enzyme α-glucan water dikinase were designed. Stable expression of the APRs in Arabidopsis (*Arabidopsis thaliana*) and maize (*Zea mays*) induced aggregation of the target proteins, giving rise to plants displaying constitutive BR responses and increased starch content, respectively. Overall, we show that the sequence specificity of APRs can be harnessed to generate aggregation-associated phenotypes in a targeted manner in different subcellular compartments. This study points toward the potential application of induced targeted aggregation as a useful tool to knock down protein functions in plants and, especially, to generate beneficial traits in crops.

In order to function properly, proteins must fold into their native structure, but protein folding is often challenged by protein misfolding and aggregation (Tyedmers et al., 2010). Although protein aggregation has long been considered as a disordered process mediated by nonspecific hydrophobic interactions, it is now understood to be a sequence-specific self-association process (Mitraki, 2010; Tyedmers et al., 2010). Indeed, both in bacterial (Sabaté et al., 2010) and mammalian systems (Rajan et al., 2001), aggregation of nonhomologous proteins has been shown to occur preferentially in distinct inclusion bodies. In vitro aggregation of protein solutions can be accelerated by seeding with preformed aggregates, and this process efficiency depends critically on the sequence homology between seed and target protein (Krebs et al., 2004; O'Nuallain et al., 2004). Self-seeding is generally several orders of magnitude more efficient than cross-seeding (Ganesan et al., 2015; Surmacz-Chwedoruk et al., 2014). Aggregation-associated human diseases, such as Alzheimer's or Parkinson's disease, are in line with this notion because the processes underlying these diseases are highly specific and characterized by the aggregation of one or a few proteins in particular tissues and cell types (Jucker and Walker, 2013).

The elucidation of the structure of amyloid-forming peptides and protein fragments has shed light on the molecular origin of the sequence specificity of protein aggregation. The amyloid structure consists of the formation of a so-called cross-β conformation, whereby the peptide backbone of the aggregate creates hydrogen bond-mediated β-strand interactions, whereas the side chains contribute to the stability of these β-strands by aligning with, and closely packing to, the identical sequence of the neighboring strand (Sawaya et al., 2007; Makin et al., 2005). The registered stacking of side chains explains the aggregation sequence specificity. Indeed, backbone interactions contribute comparatively more to the amyloid structure than to the globular protein structure (Fitzpatrick et al., 2011).

The portions of a protein sequence that are susceptible to associate into aggregates by β-strand-mediated interactions are limited to short segments, defined as aggregation-prone regions (APRs). The APRs consist of 5 to 15 amino acids in length (Rousseau et al., 2006; Goldschmidt et al., 2010) and can be identified by prediction algorithms (Fernandez-Escamilla et al., 2004). The determining role of APRs has been demonstrated by "aggregation-grafting" experiments, in which insertion of an APR of an aggregating protein into the

sequence of a nonaggregating protein results in a protein with aggregation propensity and morphology similar to those of the original protein (Ventura et al., 2004).

Application of the prediction algorithm TANGO (Fernandez-Escamilla et al., 2004) to the Arabidopsis (*Arabidopsis thaliana*) proteome revealed that 80% of the proteins contain APRs, implying that, similar to other eukaryotes, plant proteomes are also susceptible to protein aggregation (Rousseau et al., 2006). As most of the Arabidopsis proteins harbor aggregation-prone sequence segments within their primary structure and as aggregation is sequence specific, it should, in principle, be possible to induce aggregation and, subsequently, functional depletion of a protein by exposing it to a short target-specific aggregating peptide in plants. First, we tested this hypothesis by targeting proteins with kinase activity in Arabidopsis plants. We selected the cytosolic glycogen synthase kinase 3/Arabidopsis SHAGGY-like kinases (GSK3/ASKs) and the chloroplast-localized α-glucan water dikinase (GWD). Arabidopsis possesses 10 ASKs grouped into four clades (Youn and Kim, 2015) that share a 50% overall sequence identity across the whole protein. Among the ASKs, BRASSINOSTEROID INSENSITIVE2 (BIN2) was characterized as a negative regulator of BR signaling (Li and Nam, 2002; Vert and Chory, 2006; Yan et al., 2009). In addition to BIN2 and its two close homologs, BIN2-LIKE1 (BIL1) and BIL2 (clade II), at least four other ASKs redundantly convey BR signals via a mechanism similar to that of BIN2 (De Rybel et al., 2009; Kim et al., 2009; Rozhon et al., 2010).

The GWD enzyme catalyzes the phosphorylation of starch in the chloroplasts by transferring β-ATP phosphate to either the C6 or the C3 position of the glycosyl residue of amylopectin and, thus, plays an essential role in starch metabolism (Mitsui et al., 2010). The phosphate groups influence the susceptibility of the starch granules to degrading enzymes, such as β-amylases. As a result, the starch breakdown is impaired in GWD-deficient plants. In GWD-antisense potato (*Solanum tuberosum*) plants (Lorberth et al., 1998), as well as in the GWD-deficient *starch excess1* (*sex1*) mutants of Arabidopsis (Yu et al., 2001), the foliar starch content is significantly higher than that of the respective wild-type plants. In addition to the model plant Arabidopsis, we applied the APR-mediated aggregation by targeting the GWD enzyme in maize (*Zea mays*).

Our work demonstrates that overexpression of different APRs, derived from a single protein or protein family, fused to a fluorescent carrier, results in specific knockdowns similar to previously described genetic mutants. We show that direct interactions between the APRs and the target proteins caused the loss of function of the proteins. Moreover, specific subcellular targeting of the synthetic APRs can be achieved in both model and crop plant species. Hence, the APR expression approach presented here can be used as an innovative knockdown method to inactivate proteins by specific in vivo pull-down in defined subcellular compartments of plants. In addition, the results also underline that, at least in plants, protein aggregation is not cytotoxic per se, but rather that the functional effect of the aggregates observed here appear to be dominated by sequence-specific cross-seeding of the aggregation of cellular APR-sharing proteins.

RESULTS

Design of the Aggregation Constructs

To simultaneously knock out the function of all 10 ASKs in Arabidopsis by inducing specifically their misfolding and inactivation, we applied the aggregation prediction algorithm TANGO (Fernandez-Escamilla et al., 2004) to BIN2 in order to identify overlapping aggregation-prone peptides in the 10 target proteins. One APR of nine amino acids with a TANGO aggregation score greater than 50 (out of a maximum of 100) and coding for the sequence ^{249}QLVEIIKVL^{257} in BIN2 was detected (hereafter referred to as BIN2$^{249\text{-}257}$; Fig. 1A; Supplemental Table S1). The BIN2$^{249\text{-}257}$ APR was situated in the kinase domain preceding the highly

[1] This work was supported by grants from the Agency for Innovation by Science and Technology ("Strategisch Basisonderzoek" project no. 60839), Ghent University ("Industrieel Onderzoeksfonds" F2014/IOF-StarrTT261 and Multidisciplinary Research Partnership "Biotechnology for a Sustainable Economy" no. 01MRB510W), the Research Foundation-Flanders (Joint Project Bulgarian Academy of Sciences VS.025.13N), the Interuniversity Attraction Poles Program (IUAP VII/29), initiated by the Belgian State, Science Policy Office, University of Leuven, and the European Research Council under the European Union's Horizon 2020 Framework Programme (ERC Grant agreement 647458).

[2] Present address: Bekintex at Bekaert NV, 8000 Bruges, Belgium.

[3] Present address: Institute of Plant Physiology and Genetics, Bulgarian Academy of Sciences, 1113 Sofia, Bulgaria.

[4] Present address: Dana Farber Cancer Institute and the Broad Institute/MIT, Cambridge, MA, 02141.

[5] Present address: State Key Laboratory for Oncogenes and Related Genes, Division of Gastroenterology and Hepatology, Renji Hospital, Shanghai Institute for Digestive Diseases, Shanghai Jiao-Tong University School of Medicine, Shanghai 200001, China.

* Address correspondence to frederic.rousseau@switch.vib-kuleuven.be, joost.schymkowitz@switch.vib-kuleuven.be, or eugenia.russinova@psb.vib-ugent.be.

The author responsible for distribution of materials integral to the findings presented in this article in accordance with the policy described in the Instructions for Authors (www.plantphysiol.org) is Eugenia Russinova (eugenia.russinova@psb.vib-ugent.be).

D.I., F.R., J.S., and E.R. conceived the research and designed and supervised the experiments; S.C. initiated the work; C.B. designed and performed most of the experiments; I.V. provided technical assistance to C.B.; R.D.R. performed the TEM work; K.M. and M.V. did the expression studies and data analysis; S.A. and M.V.L. made transgenic maize lines; S.A., D.R., M.V.L., F.V.B., and D.I. contributed to the maize analyses; R.G., F.D.S., and J.X. performed the FTIR and expression analysis; C.B., F.R., J.S., and E.R. wrote the article with contributions of all the authors.

[OPEN] Articles can be viewed without a subscription.

www.plantphysiol.org/cgi/doi/10.1104/pp.16.00335

conserved TREE domain that plays a key role in the BIN2 function (Choe et al., 2002). Comparison of the BIN2$^{249-257}$ amino acid sequence with the Arabidopsis proteome revealed that this APR was identical to the APRs identified in 8 of 10 ASKs and differed with only one amino acid (Val-256 to Ile-256) in the APRs of the remaining two ASKs (Fig. 1A; Supplemental Table S2). For modulation of the APR aggregation properties, different synthetic aggregating blocks (SABs) were designed. Each SAB was C-terminally fused to GFP for visualization and solubility increase (Fig. 1C; Supplemental Table S3). To stimulate aggregation, the BIN2 APR was combined with a modified version of the unnatural amyloid-forming booster (B) sequence STVIIE (López De La Paz et al., 2002; BIN2$^{249-257}$B). In contrast, to slow down the aggregation of the synthetic booster by charge repulsion (Chiti et al., 2003), an Arg (R) was included on both APR flanks, thus modifying the BIN2$^{249-257}$B into BIN2$^{249-257}$RB (Supplemental Table S3). As charged residues are enriched at the flanks of APRs to decrease aggregation and function as natural "aggregation gatekeepers" (De Baets et al., 2014), five to six naturally flanking (NF) amino acids were added to the BIN2$^{249-257}$ APR and expressed, including the first six amino acids of the BIN2 protein (MADDKE) in a single copy (BIN2$^{249-257}$NF) or in tandem (T) (BIN2$^{249-257}$NFT) (Supplemental Table S3). The aim of the tandem constructs was to amplify the aggregation potential by mimicking the repeating patterns of APRs that are observed in naturally occurring functional amyloids, such as the yeast prions (Bednarska et al., 2016).

The GWD protein is encoded by a single gene in Arabidopsis and in maize. Similarly, the prediction algorithm TANGO (Fernandez-Escamilla et al., 2004) was used to identify APRs in orthologous proteins of Arabidopsis (AtGWD) and maize (ZmGWD; Supplemental Table S1). Three different APRs with a TANGO score higher than 50 were identified for each target protein in Arabidopsis and maize (Fig. 1B; Supplemental Table S1). The Arabidopsis APRs AtGWD$^{534-541}$ and AtGWD$^{821-829}$ were identical to the maize ZmGWD$^{599-610}$ and ZmGWD$^{889-897}$, respectively, whereas the APRs AtGWD$^{1227-1234}$ and ZmGWD$^{1082-1088}$ were specific for each species (Fig. 1B). Searches of the Arabidopsis proteome with the three selected GWD APRs did not reveal proteins containing identical APRs or APRs with a single mismatch (Supplemental Table S2). However, the ZmGWD$^{1082-1088}$ APR was similar to five unrelated proteins in the maize proteome (one mismatch) and was excluded from further studies.

The SABs for the GWD proteins consisted of tandem APRs flanked by the NFs of BIN2 and fused at their N terminus to a chloroplast transit peptide signal sequence for specific targeting to the chloroplasts (Supplemental Table S3) and at their C terminus to GFP or YFP when expressed in Arabidopsis and maize, respectively (Fig. 1C). The SABs AtGWD$^{534-541}$NFT, AtGWD$^{821-829}$NFT, and AtGWD$^{1227-1234}$NFT were expressed in Arabidopsis, whereas ZmGWD$^{599-610}$NFT and ZmGWD$^{889-897}$NFT were introduced into maize after codon usage optimization.

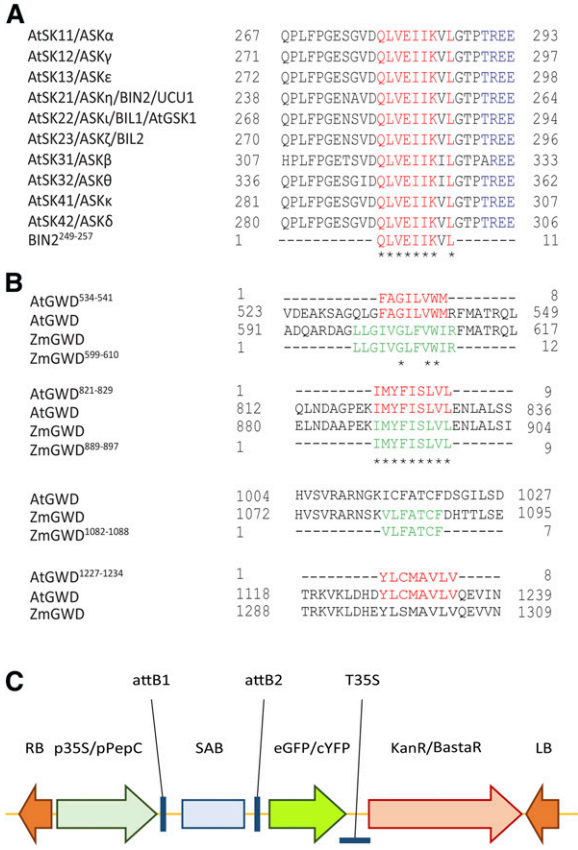

Figure 1. Selected APRs and aggregation constructs design. A, Multiple alignment of ASK amino acid sequences with the aggregating peptide BIN2$^{249-257}$. B, Multiple alignment of the APRs targeting the GWD protein in Arabidopsis (AtGWD$^{534-541}$, AtGWD$^{821-829}$, and AtGWD$^{1227-1234}$) and in maize (ZmGWD$^{599-610}$, ZmGWD$^{889-897}$, and ZmGWD$^{1082-1088}$) with their target protein, respectively. Identical residues are underlined with asterisks and indicated in red for Arabidopsis and in green for maize. The TREE kinase domain, conserved within the amino acid sequences of ASKs, is indicated in blue. Alignments were done with Clustal Omega. C, Schematic representation of constructs expressing different APR variants, indicated as SABs. SABs are fused to eGFP or cYFP at their C terminus. Only the GWD APRs were targeted to the chloroplast by adding a transit peptide at their N terminus. p35S, CaMV 35S promoter; pPePC, PepC promoter; eGFP, enhanced GFP; cYFP, citrine YFP; KanR/BastaR, kanamycin/Basta resistance gene; RB, right border; LB, left border.

In Vivo Aggregation Induced by Expression of Selected APRs in Plant Cells

All constructs, including controls, such as free GFP and booster (B)-GFP (Supplemental Table S3) were expressed transiently in leaf epidermis of tobacco (*Nicotiana benthamiana*) and stably in Arabidopsis with the constitutive cauliflower mosaic virus (CaMV) 35S promoter. Confocal fluorescence microscopy was used to evaluate the aggregation formation in the tobacco leaf epidermal cells 4 d after infiltration (Fig. 2) and in epidermal cells of roots, hypocotyls, and cotyledons of 7-d-old Arabidopsis plants grown in vitro (Supplemental Fig. S1). Consistently in both expression

systems, the SABs containing either the booster sequence in combination with the Arg-flanked APR (BIN2$^{249\text{-}257}$RB) or the tandemly repeated APRs (BIN2$^{249\text{-}257}$NFT) were the most effective in perinuclear accumulation of GFP-labeled aggregates (Fig. 2A; Supplemental Fig. S1A). In contrast, the free GFP control accumulated throughout the cytosol and inside the nucleus. The B-GFP and BIN2$^{249\text{-}257}$B-GFP fusions accumulated mainly in inclusion bodies, indicating low solubility of the aggregates, whereas the BIN2$^{249\text{-}257}$NF-GFP fusion was found predominantly in the cytosol, implying a reduced aggregation tendency (Fig. 2A; Supplemental Fig. S1A).

Transient expression of all GWD SABs in tobacco leaf epidermis resulted in aggregate formation inside the plastids, except for ZmGWD$^{1082\text{-}1088}$NFT, in which the YFP fluorescence was visible as a diffused signal in the chloroplasts (Fig. 2B). Consistently, when stably transformed in Arabidopsis plants, the AtGWD$^{534\text{-}541}$NFT and AtGWD$^{821\text{-}829}$NFT SABs, but not AtGWD$^{1227\text{-}1234}$NFT-GFP, caused the formation of GFP-labeled aggregates inside the chloroplasts in leaf epidermal and palisade cells (Supplemental Fig. S1B). The ZmGWD$^{599\text{-}610}$NFT and ZmGWD$^{889\text{-}897}$NFT SABs were stably expressed in maize under control of the maize mesophyll-specific phospho*enol*pyruvate carboxylase (PepC) promoter, previously used to down-regulate GWD only in leaves, where the enzyme is the most abundant (Sattarzadeh et al., 2010). Confocal microscopy revealed that in mesophyll cells of the third or fourth leaves of 14-d-old transgenic maize seedlings, ZmGWD$^{889\text{-}897}$NFT and ZmGWD$^{599\text{-}610}$NFT induced pronounced aggregate formation (Supplemental Fig. S1C) in the chloroplasts, as seen in the tobacco experiments.

Next, we analyzed cell extracts of transgenic Arabidopsis plants (Fig. 3, A and B) and tobacco leaves transiently expressing the GFP-tagged SABs (Supplemental Fig. S2, A and B) under nondenaturing conditions by means of Blue Native (BN)-PAGE to verify the Mr of the induced aggregates and whether the target proteins had presumably acquired a different electrophoretic mobility when a specific APR was overexpressed. The BN-PAGE analysis revealed the occurrence of high-M_r protein complexes for all SABs. Notably, the BIN2 SABs containing the booster sequence induced the highest M_r protein complexes and the APRs in tandem induced the formation of aggregates more than twice the M_r of a single APRs (Fig. 3, A and B; Supplemental Fig. S2A). Interestingly, aggregates seemed to be less abundantly induced by the expression of YFP-tagged SABs than by that of the respective GFP fusions, suggesting that the choice of the fluorescent carrier protein most probably influences protein aggregation (Supplemental Fig. S2B).

To investigate the biochemical nature of the aggregates formed in plant cells, we analyzed by means of Fourier transform infrared (FTIR) spectroscopy the high-M_r aggregates that had been immunoprecipitated with anti-GFP antibodies from lysates prepared from Arabidopsis transgenic seedlings that expressed different BIN2 SABs. For all constructs, IR absorption peaks 1620, 1635, and 1690 cm^{-1} were detected (Fig. 3C). This result supports the formation of an amyloid-like β-structure because absorbance of IR light at these wave numbers is a characteristic feature of β-structures. Transmission electron microscopy (TEM) combined with immunogold labeling of different Arabidopsis tissues expressing the BIN2 SABs with the strongest aggregation properties, namely, BIN2$^{249\text{-}257}$RB and BIN2$^{249\text{-}257}$NFT, revealed that aggregates localized in the cytosol. In the BIN2$^{249\text{-}257}$RB-producing plants, the aggregated proteins accumulated either as amorphous clusters or as more ordered and elongated fibril-like structures (Fig. 3, D and E), whereas in the BIN2$^{249\text{-}257}$NFT plants, these ordered structures were absent and free cytosolic proteins occurred most frequently (Fig. 3F). These variations in aggregate morphology reflected the differences in construct design and the impact of the strongly aggregating amyloid-forming booster sequence.

The APRs Interacted Specifically with Their Targeted Proteins in Vivo

To evaluate the specificity of the induced protein aggregations, we carried out colocalization experiments in leaf epidermal cells of tobacco between GFP-tagged ASKs (BIN2, BIL1, ASKα, ASKγ, and ASKθ) and the RFP-tagged BIN2$^{249\text{-}257}$NFT, expressed from CaMV 35S and estradiol-inducible promoters, respectively. Four days after transfection and following a 24-h induction of the BIN2$^{249\text{-}257}$NFT-RFP expression, a strong colocalization was observed between the APR and all target proteins (Supplemental Fig. S3).

The direct interaction between the BIN2$^{249\text{-}257}$ APR and each of the 10 target ASKs was confirmed by a bimolecular fluorescence complementation (BiFC) assay. Coexpression of each of the ASKs tagged with the N-terminal GFP fragment (nGFP) and the BIN2$^{249\text{-}257}$NFT tagged with the C-terminal part of GFP (cGFP) in tobacco leaves resulted in a fluorescent signal (Fig. 4A; Supplemental Table S4). The self-interaction property of the BIN2$^{249\text{-}257}$ APR was assessed by coexpressing the BIN2$^{249\text{-}257}$NFT-nGFP and BIN2$^{249\text{-}257}$NFT-cGFP constructs (Fig. 4A). In all cases, despite the observed GFP signal, no GFP-labeled aggregates were formed, probably due to the slow reassociation of the two GFP fragments that could have slowed down the aggregate formation.

Next, the hemagglutinin (HA)-tagged BIN2 was coimmunoprecipitated in all samples after transient coexpression with each BIN2$^{249\text{-}257}$ APR-containing construct in tobacco leaf epidermal cells, validating the direct interaction between BIN2$^{249\text{-}257}$ and its target protein in vivo (Fig. 4B). Remarkably, substitution of Val-251 and Ile-254 by two prolines (P) that lowers the aggregation propensity (Richardson and Richardson, 2002) in the BIN2$^{249\text{-}257}$ APR, completely abolished its

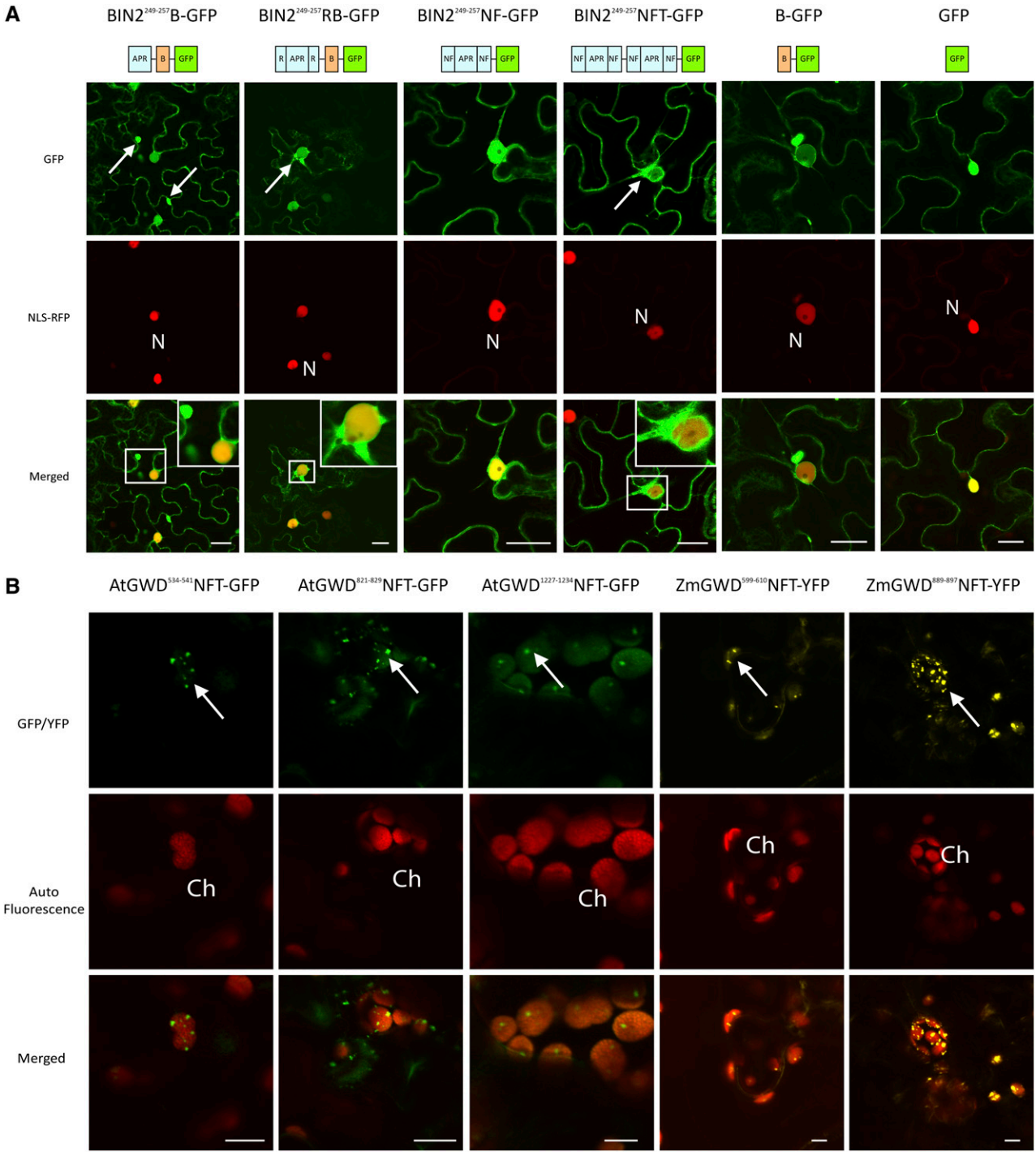

Figure 2. Subcellular localization of the APRs. A, Tobacco leaf epidermis cells transiently expressing BIN2$^{249-257}$B, BIN2$^{249-257}$RB, BIN2$^{249-257}$NF, BIN2$^{249-257}$NFT, synthetic booster (B), and free GFP coinfiltrated with a nuclear localization signal-red fluorescent protein marker (NLS-RFP). Nuclei (N) are visible in the red channel. B, Subcellular localization of AtGWD$^{534-541}$NFT-GFP, AtGWD$^{821-829}$NFT-GFP, AtGWD$^{1227-1234}$NFT-GFP, ZmGWD$^{599-610}$NFT-YFP, ZmGWD$^{889-897}$NFT-YFP, and ZmGWD$^{1082-1088}$NFT-YFP. The chlorophyll (Ch) autofluorescence is visualized in the red channel. Arrows point to aggregates labeled with GFP or YFP. Bars = 20 μm (A) and 10 μm (B).

aggregation capacity (Supplemental Tables S1–S3) and the interaction with its target protein BIN2 (Fig. 4B).

To additionally assess the specificity of the BIN2$^{249-257}$ APR for binding random proteins containing similar APR sequences, we tested the interactions between the BIN2$^{249-257}$NFT SAB and the Arabidopsis basic helix-loop-helix transcription factor MUTE (Pillitteri et al., 2007). MUTE had been identified as the only

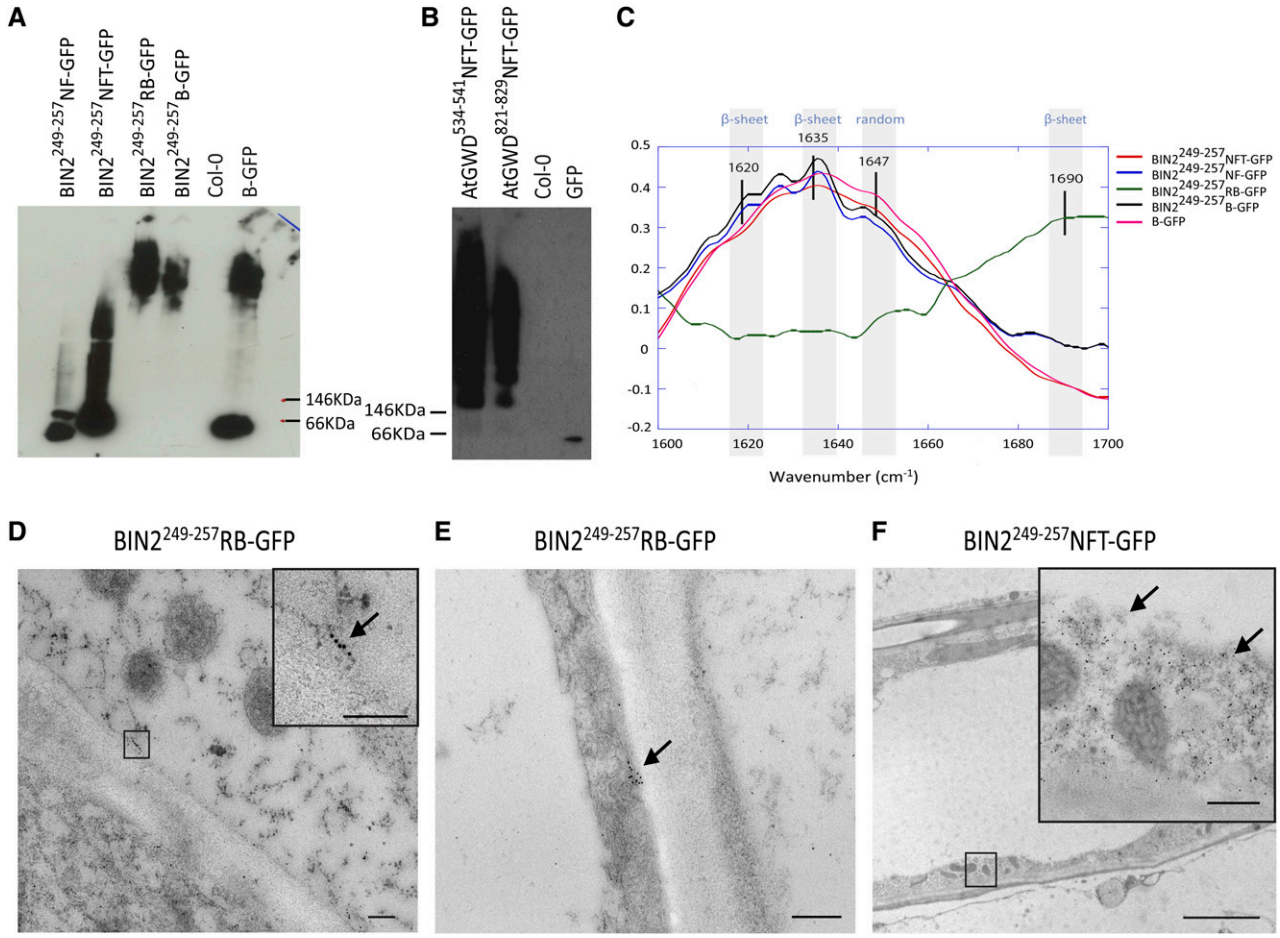

Figure 3. Expression of BIN2 and GWD APRs leading to aggregate formation. A and B, BN-PAGE and immunoblots with anti-GFP antibodies of protein aggregates induced by expression of different BIN2 (A) and GWD (B) SABs in Arabidopsis, in respect to the wild type (Col-0), booster (b)-GFP, and free GFP controls. BN-PAGE was run under nondenaturing conditions to determine the native masses of protein complexes. C, FTIR analysis of the high-M_r aggregates immunoprecipitated with anti-GFP antibodies from lysates prepared from Arabidopsis transgenic seedlings that expressed different versions of BIN2 SABs. D to F, TEM immunolocalization with anti-GFP antibodies of BIN2$^{249\text{-}257}$RB-GFP and BIN2$^{249\text{-}257}$NFT-GFP in hypocotyls (D) and in cortical cells of the root elongation zone (E and F). Ultrathin sections were poststained in uranyl acetate and lead citrate and grids were viewed with a JEM-1010 TEM (Jeol) operating at 80 kV. Bars = 0.1 (inset) and 0.5 μm in D and F, and 0.1 μm in E. Seven-day-old T3 Arabidopsis seedlings were used in all experiments. Arrows point to GFP-labeled protein aggregates.

Arabidopsis protein containing an APR that differed from BIN2$^{249\text{-}257}$ by two amino acids (Glu-252 into Lys-252 and Lys-255 into Ser-255) and had a TANGO score of 46 (Supplemental Table S2). Both BiFC and coimmunoprecipitation experiments did not reveal interactions between the BIN2$^{249\text{-}257}$ APR and the MUTE protein (Fig. 4, A and C; Supplemental Table S4). The BIN2$^{249\text{-}257}$ APR also did not interact with randomly selected, nonhomologous, and overexpressed proteins, such as the clathrin light chain (CLC) (Supplemental Fig. S4). In addition, we detected the GWD protein by means of a GWD-specific antibody after BN-PAGE of protein extracts from tobacco leaves and after immunoprecipitation with anti-GFP antibodies (Supplemental Fig. S2C). Altogether, this evidence supports the high APR specificity in target interactions.

Arabidopsis Plants Expressing an APR That Targeted the 10 ASKs Showed Weak Constitutive BR Responses

To assess whether the expression of the BIN2$^{249\text{-}257}$ APR induced loss of function of the targeted ASK proteins, we analyzed the growth and developmental phenotypes of 7-d-old in vitro- and light-grown Arabidopsis plants overexpressing the SABs with strong aggregation properties (BIN2$^{249\text{-}257}$RB and BIN2$^{249\text{-}257}$NFT). The ASK promoter-GUS studies revealed that ASKα, ASKγ, and BIN2 are the most abundantly expressed ASKs at this developmental stage (Supplemental Fig. S5) and, thus, most probably targeted ASKs by the BIN2$^{249\text{-}257}$ APR. Representative T3 homozygous transgenic lines overexpressing each BIN2$^{249\text{-}257}$RB and BIN2$^{249\text{-}257}$NFT (Supplemental Fig. S6A) displayed longer hypocotyls and roots than the wild-type control

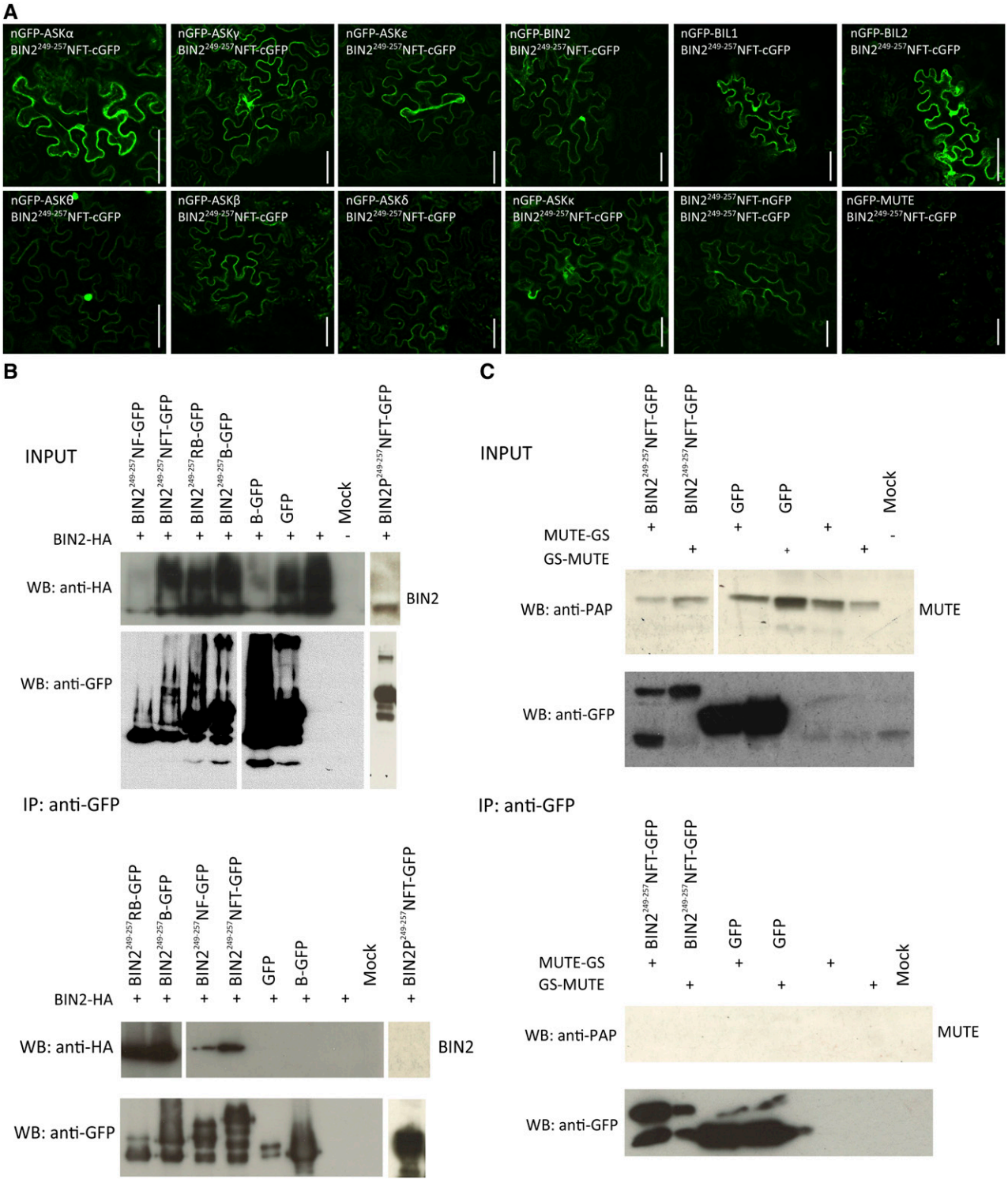

Figure 4. Specific in vivo interaction between BIN2 and the BIN2$^{249-257}$ APR. A, BiFC assay of BIN2$^{249-257}$NFT-cGFP coexpressed with different nGFP-tagged ASKs and BIN2$^{249-257}$NFT-nGFP in tobacco leaves, 3 d after infiltration. In the last panel, the interaction between BIN2$^{249-257}$NFT-cGFP and MUTE is also shown as a negative control. Bars = 50 μm. B, Coimmunoprecipitation in tobacco leaves of BIN2-HA with different BIN2$^{249-257}$ SABs after coexpression for 3 d. Booster (B)-GFP, free GFP, BIN2-HA, mock (not infiltrated leaf), and BIN2P$^{249-257}$NFT-GFP are included as negative controls. Proteins were detected with anti-HA and anti-GFP antibodies. C, Coimmunoprecipitation of BIN2$^{249-257}$NFT-GFP with MUTE-GS or GS-MUTE proteins coproduced for 3 d as in B. GFP, MUTE-GS, GS-MUTE, and mock are included as negative controls; the GS tag (consisting of a protein G tag and a streptavidin-binding peptide) reacts with the antiperoxidase (PAP) antibody. Anti-PAP and anti-GFP antibodies were used for protein detection.

Columbia-0 (Col-0; Fig. 5, A–C) and 1-month-old plants from the same transgenic lines grown in soil had larger rosettes than Col-0 (Fig. 5D). All tested transgenic lines were partially resistant to the specific BR biosynthesis inhibitor brassinazole (BRZ; Asami et al., 2000; Fig. 5E) and showed down-regulation of the BR-biosynthetic genes *CONSTITUTIVE PHOTOMORPHOGENIC DWARF* (*CPD*; Szekeres et al., 1996) and *DWARF4* (*DWF4*; Choe et al., 1998; Fig. 5F) and up-regulation of the transcription factor BRASSINAZOLE RESISTANT1 (BZR1; Wang et al., 2002). Furthermore, overexpression of the BIN2$^{249\text{-}257}$RB in a weak mutant allele of the BR receptor *bri1-5* partially rescued the mutant phenotype (Fig. 5G). These phenotypes were in line with the anticipated enhanced BR signaling due to the inactivation of the BR-negative regulators, as shown previously for the *bin2-3* knockout mutant (Yan et al., 2009).

Comparison of different tissues of wild-type and transgenic Arabidopsis plants expressing BIN2$^{249\text{-}257}$RB and BIN2$^{249\text{-}257}$NFT at the ultrastructural level indicated that the analyzed subcellular organelles, such as mitochondria and chloroplasts, were similar in terms of shape, size, and localization with those of the wild-type plants grown in vitro (Supplemental Fig. S7). In accordance, a genome-wide expression analysis revealed that only a few genes were differentially regulated (Supplemental Table S5), of which 17 were down-regulated (<0.5-fold change) and 33 were up-regulated (>1.5-fold change) in the BIN2$^{249\text{-}257}$NFT-expressing line when compared to the wild type. The changes in expression were subtle with a median increase below 2 (1.7) and gene ontology searches associated the affected genes with stress responses, hormone signaling, or chaperones. Interestingly, a 5-fold increase in the expression of the heat shock protein 70 (HSP70) was detected and later confirmed by quantitative reverse-transcription PCR (qRT-PCR) experiments (Supplemental Fig. S6B), implying that the observed aggregate formation had triggered the chaperone machinery to minimize protein aggregation. Altogether, the beneficial phenotypic traits, the plant tissue morphology, and the transcriptome data suggest that Arabidopsis plants are able to accommodate the constitutive expression of APRs without cytotoxic side effects, thus allowing the expression of aggregation-induced knockdown phenotypes.

GWD-Targeted Aggregation in Arabidopsis and Maize

In order to prove that the targeted protein aggregation is usable for proteins with different functions and subcellular localizations, Arabidopsis plants expressing AtGWD$^{534\text{-}541}$NFT and AtGWD$^{821\text{-}829}$NFT SABs fused to GFP and designed to target the AtGWD protein (Fig. 1B; Supplemental Table S3) were evaluated for loss-of-function phenotypes and compared with the known Arabidopsis GWD mutant *sex1-5* (Yu et al., 2001). The AtGWD$^{1227\text{-}1234}$NFT-expressing plants were not analyzed because of lack of GFP fluorescence. T3 homozygous transgenic lines, each overexpressing AtGWD$^{534\text{-}541}$NFT or AtGWD$^{821\text{-}829}$NFT (Supplemental Fig. S6C), were grown in soil for 6 weeks. The rosettes of AtGWD$^{821\text{-}829}$NFT-expressing plants were smaller than those of the wild type and comparable to those of the *sex* mutants (Fig. 6, A and B). In agreement with the phenotypic observations, a significant increase in starch content in the fourth and fifth leaves of 6-week-old Arabidopsis plants was detected by means of an iodine staining only in the line overexpressing the AtGWD$^{821\text{-}829}$NFT-GFP construct (Fig. 6, C and D).

T2 transgenic maize plants (Fig. 7) overexpressing ZmGWD$^{599\text{-}610}$NFT-YFP and ZmGWD$^{889\text{-}897}$NFT-YFP proteins (Supplemental Fig. S6D) that had been predicted to aggregate the maize GWD ortholog were evaluated for growth phenotypes and starch content. At least two segregating T2 transgenic lines per construct were analyzed. Eight-week-old mature plants from both lines showed mild growth retardation phenotypes in comparison to the B104 wild-type control when grown in the greenhouse (Fig. 7). Iodine staining of 10 leaf disks from the mature zone (Nelissen et al., 2012) of leaf 7 to leaf 10, collected at approximately 3 cm distance from each other, revealed a 10% starch increase in leaf 8 and leaf 9 of plants expressing ZmGWD$^{599\text{-}610}$NFT-YFP and approximately 8% in leaf 9 and 10 of plants expressing ZmGWD$^{889\text{-}897}$NFT-YFP (Fig. 7B; Supplemental Fig. S8).

DISCUSSION

Here, we demonstrated the potential of targeted aggregation to specifically down-regulate a protein function in plants without affecting the cellular viability and the overall plant fitness. The proposed method is based on the fact that protein aggregation is often mediated by short aggregation-prone segments of polypeptide chains that become exposed upon misfolding, leading to their assembly into intermolecular aggregates. Overall, this self-assembly process has been shown to be remarkably specific because most proteins are unable to coaggregate and protein deposits in patients affected by neurodegenerative diseases are highly enriched in one particular protein (Rajan et al., 2001; Ren et al., 2009).

Although aggregate formation has been observed in bacteria, fungi, insects, invertebrates, and humans, in which it is usually associated with numerous diseases, this process is most probably ubiquitous across all the kingdoms, including plants. The aggregation propensity of the complete Arabidopsis proteome, analyzed by the protein aggregation prediction algorithm TANGO, was similar to that of other eukaryotes: 12% of the Arabidopsis proteome possesses a significant aggregation tendency versus 11.3% of the human proteome (Rousseau et al., 2006), suggesting that plants can be an attractive model to study protein aggregation. We show that it is possible to induce targeted aggregation of selected proteins in different locations in the plant cell and in different plant species. Our results indicate

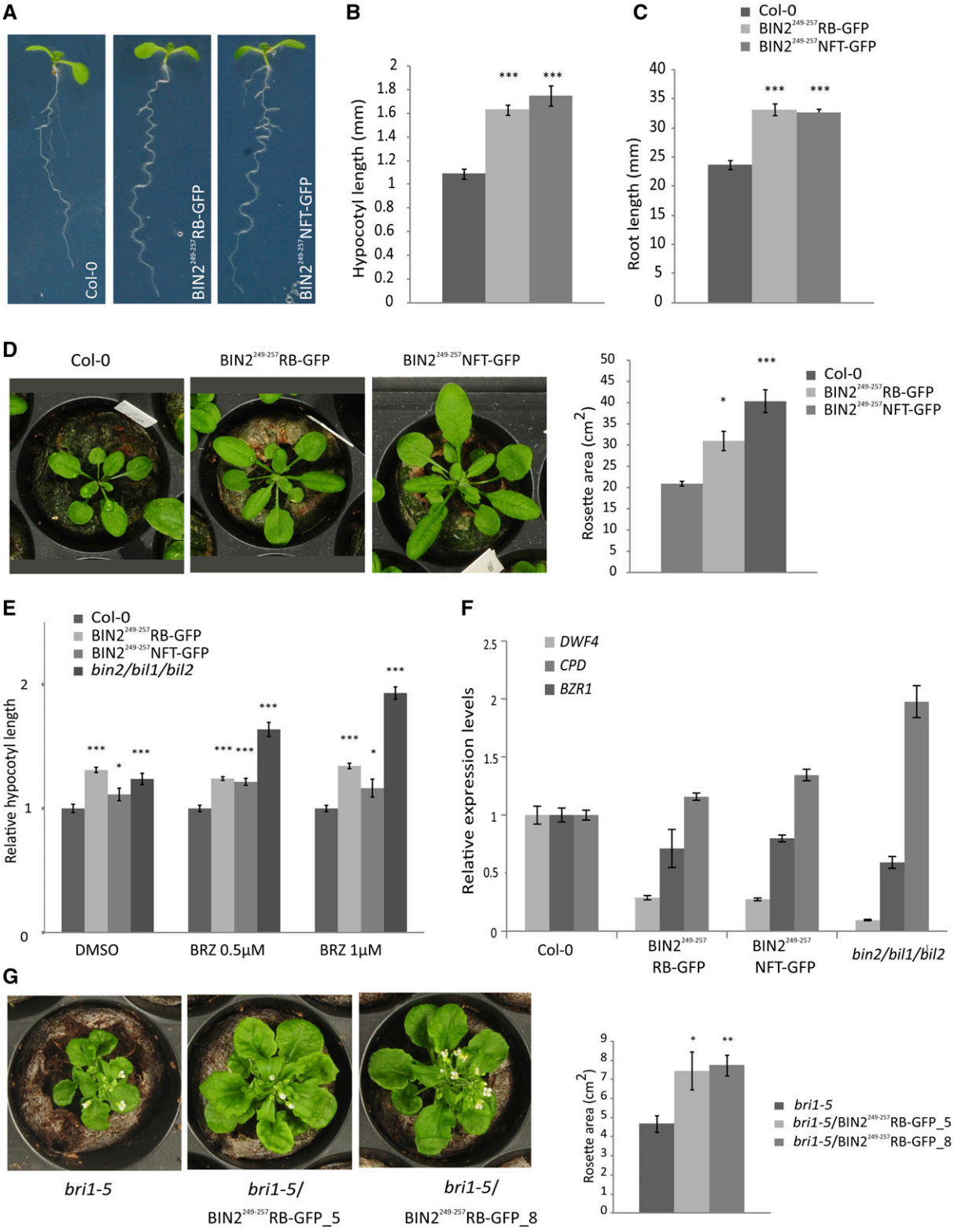

Figure 5. Constitutive BR responses in Arabidopsis plants expressing the BIN2 APR. A, Seven-day-old in vitro-grown Arabidopsis wild-type (Col-0) and T3 transgenic plants expressing BIN2$^{249\text{-}257}$RB and BIN2$^{249\text{-}257}$NFT. B and C, Hypocotyl and root length measurements of the plants shown in A ($n > 15$). D, Rosettes and rosette area quantification of the lines shown in A and grown in soil for 30 d ($n = 8$). E, Hypocotyl lengths, relative to Col-0, of BIN2$^{249\text{-}257}$RB, BIN2$^{249\text{-}257}$NFT, and *bin2/bil1/bil2* seedlings grown in the dark for 5 d on medium containing DMSO or 1 μM BRZ ($n > 15$). F, Relative expression of *DWF4*, *CPD*, and *BZR1* genes in

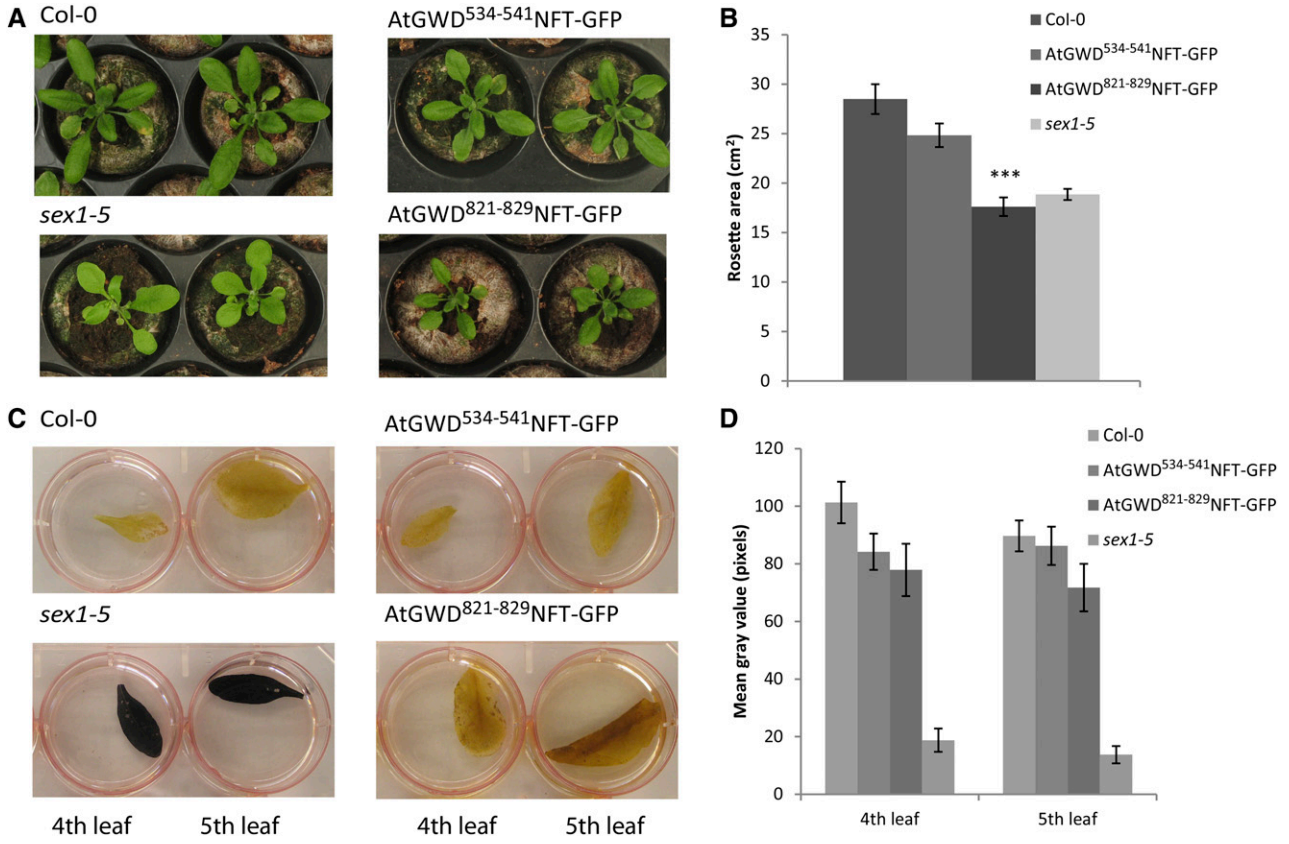

Figure 6. GWD-targeted aggregation in Arabidopsis. A and B, Phenotypes and rosette area quantification ($n = 10$) of 6-week-old Arabidopsis T3 transgenic plants expressing AtGWD$^{534-541}$NFT-GFP and AtGWD$^{821-829}$NFT-GFP, respectively. The wild type (Col-0) and *sex1-5* mutant were used as controls ($n = 10$). C and D, Lugol staining and intensity color quantification of the 4th and 5th leaves from 6-week-old Arabidopsis T3 transgenic plants shown in A. The Lugol staining intensities are shown as grey values in pixels, with the values 0 and 250 pixels for black and white for 8-bit images, respectively ($n = 4$). Error bars represent SD, ***$P<0.0001$ (Student's *t*-test). n, Number of plants analyzed.

that the overexpression of APRs with a predicted high aggregation potential can trigger misfolding and subsequent aggregation of the endogenous proteins (e.g. ASKs and GWD), resulting in a conditional loss of their activity and leading to constitutive BR responses and increased amounts of starch, respectively. Thus, our data demonstrate that the coaggregation of polypeptides in plant cells also depends on the involvement of a short aggregation-nucleating region. The process of targeted aggregation shares similarities with the functional regulation of yeast prions, although important differences should be noted.

Both yeast prion formation and targeted aggregation of ASKs or GWD appear to be governed by protein-specific aggregation without overall cell toxicity. This notion is supported by the observed phenotypes with an increased plant biomass and lack of defects at the ultrastructural level in various subcellular organelles, such as mitochondria and chloroplasts, for the ASK plants that overexpress APRs. In addition, a genome-wide expression study of these plants revealed very subtle changes in gene expression. The 5-fold increase of the *HSP70* expression is most probably an adaptive change to the proteostatic network rather than a strong stress response. Although previous expression profile analyses of the Arabidopsis *HSP70* genes have shown that these chaperones are indeed overexpressed in response to environmental stresses, such as heat, drought, and chemical treatments, the amplitude of the *HSP70* up-regulation in these experiments ranged between a 15- to 20-fold change (Sugio et al., 2009). In addition, a high overexpression of the major cytosolic

Figure 5. (*Continued.*)
7-d-old Col-0, BIN2$^{249-257}$RB, BIN2$^{249-257}$NFT, and *bin2/bil1/bil2* seedlings. G, Phenotypes and rosette area quantification of 30-d-old *bri1-5* and two independent *bri1-5*/BIN2$^{249-257}$RB T3 line 5 and line 8 ($n = 8$). Error bars represent SD, *$P<0.05$, **$P<0.001$, and ***$P<0.0001$ (Student's *t*-test). N, number of plants analyzed.

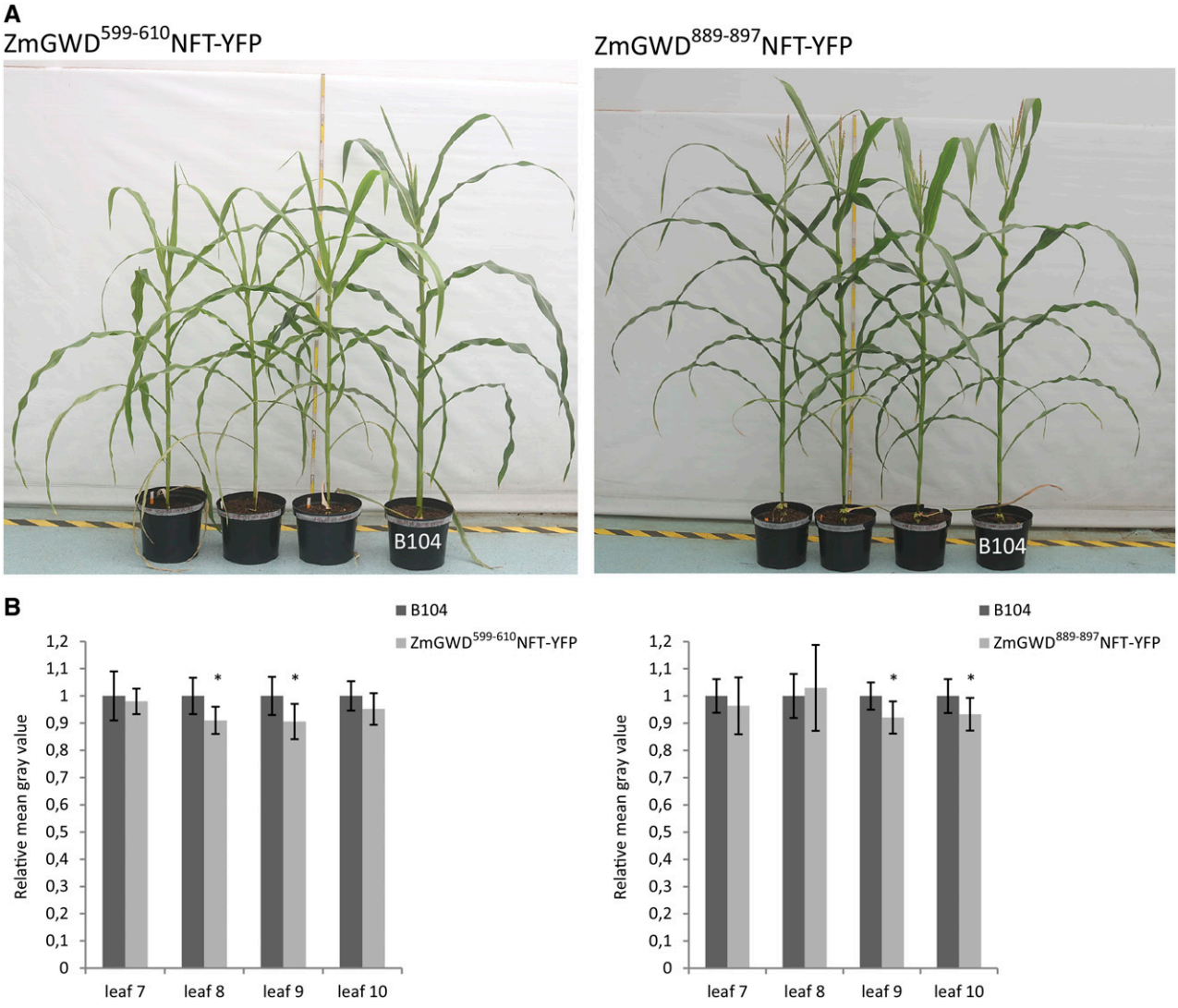

Figure 7. GWD-targeted aggregation in maize. A, Phenotypes of 80-d-old T2 segregating maize lines expressing ZmGWD$^{599-610}$NFT-YFP or ZmGWD$^{889-897}$NFT-YFP from the mesophyll-specific promoter (pPePC) and compared with the wild-type control (B104). B, Lugol staining quantifications of mean gray values of leaf 7 to10 in plants shown in Supplemental Fig. S8, A and B. The Lugol staining intensities are presented as relative grey values. Error bars represent SD, *$P<0.05$ (Student's *t*-test).

HSP70 in Arabidopsis had negative consequences for plant growth and viability (Sung and Guy, 2003). In contrast, no changes were observed in root growth. The profile of the transcriptional features of the responses to misfolded protein accumulation due to heat stress in the cytosol has revealed that the overall number of genes affected is much higher (2696 genes; Sugio et al., 2009) than that in our study (39 genes), hence excluding any proteotoxic effect generated by the overexpression of the APRs.

Moreover, threshold effects were detected for the functional knockout of the selected proteins. Plants that displayed obvious ASK knockdown phenotypes accumulated perinuclear aggregates marked by GFP fluorescence (Fig. 2A; BIN2$^{249-257}$RB and BIN2$^{249-257}$NFT), as previously shown in yeast and mammalian cells (Kaganovich et al., 2008). When GFP was visible in inclusion bodies (Fig. 2A; BIN2$^{249-257}$B), indicative of low aggregate solubility, no phenotypes were observed, similarly to the cytoplasmic APRs (Fig. 2A; BIN2$^{249-257}$NF). In the case of the GWD protein, different APRs were tested in Arabidopsis and in maize. Likewise to the BIN2 knockdown, GWD loss-of-function phenotypes were generated with the APRs capable to form GFP-labeled aggregates inside the chloroplasts. Interestingly, the level of overexpression of the APRs and their protein knockdown capacities did not correlate. Overall, the APR-generated phenotypes were weaker than those of the known genetic mutants. When applied to multiple gene families, the efficiency of the targeted

aggregation is most probably limited by the expression pattern of each gene member, the protein turnover, and the successful delivery of the APR to the respective targets. Therefore, tissue- and cell-specific promoters and specific sequences are essential to target the APRs to cellular organelles, as is the case for GWD.

We demonstrated that the target-specific APRs can be used to selectively knockdown proteins in plants. Our results show that APRs with similar TANGO scores (49–52) and high sequence identity (89%, one mismatch) can bind the target proteins, whereas an APR with a TANGO score of 46, but bearing two mismatches (78% sequence identity), displayed a interaction loss. A complete lack of interaction was also observed when Val-251 and Ile-254 in the BIN2 APR were substituted by Pro that drastically reduces the aggregation propensity by breaking the β-strand structure (Richardson and Richardson, 2002) and, thus, lowers the TANGO score to 0, even with maintenance of the sequence identity (78%). In general, our data are in agreement with previous studies in which the specificity of APR-mediated interactions is determined by the combination of aggregation propensity and sequence matching (Ganesan et al., 2015).

Besides its use as protein function-suppressing method, our approach emerges as a powerful tool to study protein aggregation mechanisms. Aggregation is often examined in the context of human diseases, in which aggregation of particular proteins is generally linked to lethal phenotypes. Virtually nothing is known about the mechanisms that control the self-assembly of proteins into aggregates in plants. The FTIR spectroscopy supports the hypothesis that β-sheet-containing aggregates are induced by the overexpression of the selected APRs. In addition, TEM combined with immunogold APR labeling in different Arabidopsis tissues has revealed that aggregated proteins accumulate both as amorphous clusters and as more ordered and elongated fibril-like structures, suggesting that aggregate formation in plants might differ from the known amyloid formation in mammalian cells.

Overall, our data show that endogenous production or artificial introduction into a cell of small peptides with the APRs of a targeted protein will provide the opportunity to generate highly specific protein knockdowns posttranslationally in different plant species. This method has several potential advantages in respect to known knockdown approaches that act at the genomic or transcriptional level, such as T-DNA or transposon insertions and RNA-mediated gene suppression (RNA interference [RNAi], artificial microRNA, and antisense RNA) that can often suffer from significant drawbacks, such as off-target effects or systemic silencing. Additionally, sensitivity to environmental and developmental stresses and the observed trait instability also affect the efficiency of the RNA-silencing technology (Small, 2007; Frizzi and Huang, 2010). The APR peptides can also be expressed over several generations without silencing, therefore overcoming the phenotypic instability of the RNAi technology.

As the synthetic APR-containing peptides can be targeted to different cellular compartments or be secreted in the apoplast, protein knockdowns with high selectivity can be obtained. The latter might generate the development of a knockdown strategy with applications in crop protection, when RNAi has failed to induce resistance against a number of pathogens (Price and Gatehouse, 2008). In comparison to the antibody-based technology, in which the produced recombinant proteins can have a low activity due to incorrect folding and often have low product yields and recovery problems (Ahmad et al., 2012), the intrinsic nature of the APRs to form β-sheet structures assures their structural stability when overexpressed in cells.

MATERIALS AND METHODS

In Silico Analysis

Multiple sequences of ASKs and $BIN2^{249\text{-}257}$ APR were aligned with the Clustal Omega program (Sievers et al., 2011), as well as $AtGWD^{534\text{-}541}$, $AtGWD^{821\text{-}829}$, $AtGWD^{1227\text{-}1234}$, $ZmGWD^{599\text{-}610}$, $ZmGWD^{889\text{-}897}$, and $ZmGWD^{1082\text{-}1088}$ APRs against their corresponding target protein fragments in AtGWD and ZmGWD sequences. The *GWD* gene of maize (*Zea mays*; GRMZM2G412611, UniProtKB annotation, A0A096TN87), orthologous to that of Arabidopsis (*Arabidopsis thaliana*; At1g10760) was identified with the PLAZA2.5 bioinformatics platform (Proost et al., 2009). The aggregation propensity of the GSK3/ASK proteins was calculated with the algorithm TANGO (Fernandez-Escamilla et al., 2004) that predicts aggregation-nucleating sequences in proteins. To ensure the discovery of all sequences matching a given APR within a certain number of mutations, we used an exhaustive algorithm that compares the APR sequence to all possible fragments of the same size in the proteome (Ganesan et al., 2015).

Plant Material, Growth Conditions, and Plasmid Engineering

Arabidopsis accessions Col-0 or Wassilewskija (Ws-2) and maize B104 inbred line (Hallauer et al., 1997) were used for transformation and 4-week-old *Nicotiana benthamiana* plants for leaf infiltration experiments. The *bin2/bil1/bil2*, *bri1-5*, and *sex1-5* mutant lines had been described previously (Vert and Chory, 2006; Noguchi et al., 1999; Yu et al., 2001).

The *ASK*, *MUTE*, and *CLC* genes and the $BIN2^{249\text{-}257}$, $BIN2P^{249\text{-}257}$, $AtGWD^{534\text{-}541}$, $AtGWD^{821\text{-}829}$, $AtGWD^{1227\text{-}1234}$, $ZmGWD^{599\text{-}610}$, and $ZmGWD^{889\text{-}897}$ sequences (Supplemental Table S6) were cloned in the pDONR221 vector (Invitrogen) and ASKs and PepC promoters in pDONR-P4P1 via Gateway cloning (Invitrogen). The PepC promoter sequence was derived from the pPTN512 vector (Sattarzadeh et al., 2010). The CaMV 35S promoter containing pEN-L4-2-R1 (Karimi et al., 2007) was also used, whereas the pEN-R2-F-L3 (Karimi et al., 2007), pEN-R2-citrineYFP-L3 (kind gift from Hilde Nelissen), and pDONR-P2R-TagRFP-P3 (Merzlyak et al., 2007) entry clones were used to generate translational fusions to GFP, YFP, or RFP in the pK7FWG2, pK7m34GW, pBb7m34GW, or pH7m34GW destination vectors (Karimi et al., 2007). For MUTE-GS fusions, the pDONR221-expressing *MUTE* (At3g06120) was fused N-terminally rather than C-terminally to the GS Rhino tag. For the N-terminal fusions, pDONR221-MUTE was cloned into the pkNGSrhino destination vector (Van Leene et al., 2015). For the C-terminal fusions, pDONR221-MUTE was recombined with pDONR-P2R-GSRhino-P3 and pDONR-P4-35S-P1 donor vectors (Van Leene et al., 2015). For BIN2-HA fusions, a pKm43GW destination vector (Karimi et al., 2007) was used overexpressing (CaMV 35S promoter) the *BIN2* gene fused to 3× HA tag. The estradiol-inducible $BIN2^{249\text{-}257}$NFT-RFP construct was engineered with the pMDC7-m13GW destination vector (Curtis and Grossniklaus, 2003). The sequence of the chloroplast transit peptide signal from the small ribulose-1,5-biphosphate carboxylase/oxygenase subunit of pea (*Pisum sativum*; Bowler et al., 1991; Supplemental Table S6) was included at the 5′ of the $AtGWD^{534\text{-}541}$, $AtGWD^{821\text{-}829}$, $AtGWD^{1227\text{-}1234}$, $ZmGWD^{599\text{-}610}$, and $ZmGWD^{889\text{-}897}$ sequences. The ASK promoter sequences were recombined into the pMK7S*NFm14GW vector (Karimi et al., 2007) to generate transcriptional

fusions to a nuclear localization signal (NLS)-GFP-GUS, of which the *pBIN2::NLSGFP-GUS* construct had been described previously (Gudesblat et al., 2012). For the BiFC experiments, $BIN2^{249-257}$NFT, ASKs, and MUTE were fused to the N or C terminus of GFP fragments (nGFP or cGFP) as described (Boruc et al., 2010). As negative controls, constructs overexpressing nGFP or cGFP were used. Codon usage was optimized for the expression in Arabidopsis and maize. The resulting expression clones were transformed into *Agrobacterium tumefaciens* for plant transformation. For transient expression experiments, the abaxial sides of 4-week-old tobacco leaves were infiltrated with *A. tumefaciens* strains cultivated with the virulence gene activator acetosyringone as described (Boruc et al., 2010). For estradiol inductions, tobacco leaves were reinfiltrated with 20 μM estradiol 3 d after injection and imaged 24 h after induction with the ImageJ software (http://rsb.info.nih.gov/ij/).

Arabidopsis seeds were stratified in the dark at 4°C for 2 d and germinated on half-strength Murashige and Skoog (MS) medium (1% [w/v] Suc) under long-day (16 h light/8 h dark) conditions at 20 to 22°C before transfer to soil. BRZ and estradiol were purchased from TCI Europe and Sigma-Aldrich, respectively. For the GUS activity analysis, 7-d-old Arabidopsis seedlings were processed as reported (Zhiponova et al., 2013).

For maize transformation, immature embryos of the B104 inbred line were cocultivated for 3 d with *A. tumefaciens* EH101 containing the ZmGWD constructs in plasmid pBb7m34GW (Coussens et al., 2012). Cocultivated embryos were cultured in the dark for 1 week on nonselective medium and transformed embryogenic callus was selected for 10 weeks on phosphinothricin-containing medium. Transgenic rooted (T0) plantlets were induced in light on regeneration medium. The presence of the transgene was confirmed by PCR and a commercial phosphinothricin activity assay (TraitChek Crop and Grain Test Kit; Strategic Diagnostic) was used to test the selection marker activity. Transgenic T0 plants were grown to maturity in the greenhouse, back-crossed (BC) to the wild type B104. BC progenies were harvested and analyzed (T1). BC of T0 plants to the wild type B104 in a reciprocal way was done to secure sufficient transgenic T1 seed production. T1 plants were grown to maturity and self-fertilized. The resulting T2 seeds were also germinated and analyzed. The primers used are presented in Supplemental Table S4.

Phenotype Analysis

Root and hypocotyl lengths of vertically grown 7-d-old seedlings were measured with the ImageJ software (http://rsb.info.nih.gov/ij/). Rosette leaf areas were calculated with ImageJ on 5- to 6-week-old Arabidopsis plants grown in soil. Means and standard deviations were calculated with the Excel 2010 software and the statistical significance by the *P* values of a two-tailed Student's *t* test. For maize, the pictures of approximately 80-d-old T2 plants were taken during anthesis and compared to untransformed plants from each transformation event.

For qualitative starch analyses, nonsenescent foliar tissues were boiled in 80% ethanol to remove chlorophyll and subsequently stained with Lugol iodine solution (Sigma-Aldrich). For Arabidopsis, the fourth and the fifth leaves of 6-week-old plants were taken, whereas for maize, 10 leaf disks per leaf, in leaves 7 to 10 of 8-week-old T2 segregating plants, were collected starting approximately 45 cm from the tip (punch number 1) until about 12 cm from the leaf base, keeping a distance of approximately 3 cm between each punch.

For Lugol staining quantifications of starch, mean gray values in pixels were measured in 8-bit RGB images with the Image J software. A fixed area was measured for each leaf sample, setting the scale in pixels and to 0. In 8-bit images, the grayscale goes from a minimum value of 0 pixel (black) to a maximum value of 250 pixel (white).

qRT-PCR and Microarray

For qRT-PCR analyses, cDNA was prepared from 1 μg of total RNA extracted in technical triplicates from 7-d-old Arabidopsis seedlings or from 30-d-old maize leaf material from the mature zone (Nelissen et al., 2012) with the RNeasy Kit (Qiagen); qRT-PCR was run on a LightCycler 480 apparatus (Roche Diagnostics) with the SYBR Green I Master kit (Roche Diagnostics) or on a MyIQ cycler with the TaqMan master mix (Bio-Rad). Targets were quantified with specific primer pairs (Supplemental Table S6). Data were analyzed with the Biogazelle qBASEplus software (Hellemans et al., 2007) with the translation initiation factor elongation factor 1-α (EF1A), cyclin-dependent kinase A (CDKA;1), ubiquitin (UBQ), and heat shock factor 1 (HSF1) as reference genes. For maize, 18S rRNA (18S) was used as reference gene.

For microarray analyses, 7-d-old seedlings of Arabidopsis Col-0 and expressing $BIN2^{249-257}$NFT-GFP were grown vertically on half-strength MS medium. Total RNA was extracted from shoot material with TRIzol (Invitrogen) and further purified with the RNeasy Kit (Qiagen). Per array, 200 μg was used to hybridize the Arabidopsis ATH1 GeneChips (Affymetrix) at the VIB Nucleomics Core Facility (Leuven, Belgium; www.nucleomics.be) according to the manufacturer's instructions. Raw data were processed with the RMA algorithm (Irizarry et al., 2003) within BioConductor with the ATH1-121501 chip definition file (www.bioconductor.org) to assign probes to genes, followed by a one-way ANOVA on all genes in parallel. *P* values were calculated with GenStat (Payne, 2012) and subsequently transformed into false discovery rates (Storey and Tibshirani, 2003) to identify differentially expressed genes.

Microscopy

Images of GUS-stained seedlings were taken with a MZ16 binocular microscope (Leica) and a Nikon 198 camera. Seven-day-old Arabidopsis seedlings and tobacco leaves were analyzed 3 to 4 d after injections with a FluoView1000 (Olympus) inverted confocal microscope equipped with a 63× water-corrected objective. Images were captured at 488- and 559-nm laser excitation and 500- to 550-nm and 570- to 670-nm long-pass emission filters for GFP and RFP, respectively. Emission fluorescence was captured in the frame-scanning mode and images were analyzed with the FluoView FV1000 software (Olympus). Intensity correlation analysis and Manders' overlap coefficient calculations were done as described (Scacchi et al., 2009) by means of an ImageJ plug-in (http://wwwfacilities.uhnresearch.ca/wcif/imagej/colour_analysis.htm). For the BiFC experiments, the autofluorescence background level measured in tobacco leaves coexpressing the cGFP and nGFP constructs was used to set the GFP signal threshold. Combinations were scored as positive interactions when the GFP signal was higher than the threshold.

For the morphological studies with TEM, fragments (1–2 mm^2) of cotyledons, hypocotyls, and roots of 7-d-old $BIN2^{249-257}$NFT-GFP and $BIN2^{249-257}$RB-GFP, plants were embedded in Spurr's resin as described (Betti et al., 2012). For immunocytochemical detection, the tissue fragments were infiltrated at 4°C in LR-White hard grade (London Resin) and immunolabeled with an anti-GFP antibody (AbCam) and secondary colloidal gold-protein A conjugates, PAG10nm (Cell Biology Department, Utrecht University) as described (Betti et al., 2012). Ultrathin sections were poststained at 20°C for 40 min in uranyl acetate and 10 min in lead citrate with an automatic contrasting system (EM AC20; Leica). Grids were viewed with a JEM-1010 TEM (JEOL) operating at 80 kV.

Protein Extraction, Pull-Down, and Immunoblots

To extract proteins for SDS-PAGE, flash-frozen 7-d-old Arabidopsis seedlings or tobacco leaves were ground and homogenized in ice-cold extraction buffer (50 mM Tris-HCl, pH 7.5, 150 mM NaCl, 1% [v/v] NP-40, 0.1% [v/v] SDS, 0.1% Na-deoxycholate, 5 mM DTT, and Complete protease inhibitor [Roche Diagnostics]). The homogenate was centrifuged at 14,000*g* twice for 20 min at 4°C and protein concentration was determined with Quick Start Bradford 1× dye reagent (Bio-Rad). Approximately 60 μg of total protein was separated on a 12% SDS-PAGE gel and transferred to polyvinylidene fluoride membranes (GE Healthcare). For pull-down experiments, proteins were extracted from flash-frozen tobacco leaves and immunoprecipitated with GFPTrap-A beads (Chromotek) as described (Roux et al., 2011).

For BN-PAGE, total proteins were extracted from flash-frozen 7-d-old Arabidopsis seedlings or tobacco leaves, separated on Novex gels (Invitrogen), and transferred to polyvinylidene fluoride membranes as described (Xu et al., 2011). For immunodetection, mouse anti-GFP (JL-8, Living Colors; Clontech), rat anti-HA (Roche Diagnostics), mouse antiperoxidase (PAP; ab21867; AbCam), or rabbit anti-GWD antibodies (kind gift of Prof. Jeorg Fettke) were used as primary antibodies at 1:5,000 or 1:1,000 dilutions. Secondary anti-mouse, anti-rat, or anti-rabbit antibodies (GE Healthcare) were used at 1:10,000 dilutions. The proteins were detected by ECL (Perkin-Elmer).

FTIR Spectroscopy

FTIR was done on a Tensor 37 FT-IR spectrometer equipped with a BioATR II cell (Bruker) as described (Xu et al., 2011).

Accession Numbers

Sequence data from this article can be found in the GenBank/EMBL data libraries, in the Arabidopsis information Resource or in the Maize Genetics and

Genomics databases under accession numbers: At4g18710 (BIN2/ASKη), At5g26751 (ASKα), At3g05840 (ASKγ), At5g14640 (ASKε), At2g30980 (BIL1/ASKζ), At1g06390 (BIL2/ASKι), At4g00720 (ASKθ), At3g61160 (ASKβ), At1g09840 (ASKκ), At1g57870 (ASKδ), At1g10760, (GWD), At3g06120 (MUTE), At2g2060 (CLC) and GRMZM2G412611 (ZmGWD).

Supplemental Data

The following materials are available.

Supplemental Figure S1. Subcellular localization of the aggregates.

Supplemental Figure S2. Biochemical analysis of the aggregates.

Supplemental Figure S3. Colocalization analysis.

Supplemental Figure S4. Absence of CLC binding by the BIN2 APR.

Supplemental Figure S5. ASK promoter-GUS expression patterns.

Supplemental Figure S6. Expression analysis of the transgenic lines.

Supplemental Figure S7. TEM analysis.

Supplemental Figure S8. Starch content analysis of the transgenic maize lines.

Supplemental Figure S9. Full scans of blots.

Supplemental Table S1. TANGO analysis.

Supplemental Table S2. PepMatch results for selected APRs.

Supplemental Table S3. Aggregation constructs design.

Supplemental Table S4. Protein-protein interactions tested by bimolecular fluorescence complementation (BiFC).

Supplemental Table S5. Microarray gene expression analysis.

Supplemental Table S6. Sequence information.

ACKNOWLEDGMENTS

We thank Carina Braeckman for Arabidopsis transformation, Griet Coussens and Leen Vercruysse for maize transformation, Wilson Ardiles for sequencing support, Thao Bui Puong, Marieke Lippens, and Anaxi Houbaert for technical help, Jacinte Beerten for assistance with TEM, Mansour Karimi for cloning the pPepC sequence in the Gateway entry vector, Hilde Nelissen for the pEN-R2-citrineYFP-L3 vector, Daniël Van Damme for the 35S::CLC-HA construct, the VIB Nucleomics Core facility for microarray experiments, Prof. Joerg Fettke for the anti-GWD antibody, and Martine De Cock for help in preparing the manuscript

Received March 8, 2016; accepted April 29, 2016; published May 4, 2016.

LITERATURE CITED

Ahmad P, Ashraf M, Younis M, Hu X, Kumar A, Akram NA, Al-Qurainy F (2012) Role of transgenic plants in agriculture and biopharming. Biotechnol Adv **30:** 524–540

Asami T, Min YK, Nagata N, Yamagishi K, Takatsuto S, Fujioka S, Murofushi N, Yamaguchi I, Yoshida S (2000) Characterization of brassinazole, a triazole-type brassinosteroid biosynthesis inhibitor. Plant Physiol **123:** 93–100

Bednarska NG, van Eldere J, Gallardo R, Ganesan A, Ramakers M, Vogel I, Baatsen P, Staes A, Goethals M, Hammarström P, et al (2016) Protein aggregation as an antibiotic design strategy. Mol Microbiol **99:** 849–865

Betti C, Lico C, Maffi D, D'Angeli S, Altamura MM, Benvenuto E, Faoro F, Baschieri S (2012) *Potato virus X* movement in *Nicotiana benthamiana*: new details revealed by chimeric coat protein variants. Mol Plant Pathol **13:** 198–203

Boruc J, Mylle E, Duda M, De Clercq R, Rombauts S, Geelen D, Hilson P, Inzé D, Van Damme D, Russinova E (2010) Systematic localization of the Arabidopsis core cell cycle proteins reveals novel cell division complexes. Plant Physiol **152:** 553–565

Bowler C, Slooten L, Vandenbranden S, De Rycke R, Botterman J, Sybesma C, Van Montagu M, Inzé D (1991) Manganese superoxide dismutase can reduce cellular damage mediated by oxygen radicals in transgenic plants. EMBO J **10:** 1723–1732

Chiti F, Stefani M, Taddei N, Ramponi G, Dobson CM (2003) Rationalization of the effects of mutations on peptide and protein aggregation rates. Nature **424:** 805–808

Choe S, Dilkes BP, Fujioka S, Takatsuto S, Sakurai A, Feldmann KA (1998) The *DWF4* gene of Arabidopsis encodes a cytochrome P450 that mediates multiple 22α-hydroxylation steps in brassinosteroid biosynthesis. Plant Cell **10:** 231–243

Choe S, Schmitz RJ, Fujioka S, Takatsuto S, Lee M-O, Yoshida S, Feldmann KA, Tax FE (2002) Arabidopsis brassinosteroid-insensitive *dwarf12* mutants are semidominant and defective in a glycogen synthase kinase 3β-like kinase. Plant Physiol **130:** 1506–1515

Coussens G, Aesaert S, Verelst W, Demeulenaere M, De Buck S, Njuguna E, Inzé D, Van Lijsebettens M (2012) *Brachypodium distachyon* promoters as efficient building blocks for transgenic research in maize. J Exp Bot **63:** 4263–4273

Curtis MD, Grossniklaus U (2003) A gateway cloning vector set for high-throughput functional analysis of genes in planta. Plant Physiol **133:** 462–469

De Baets G, Van Durme J, Rousseau F, Schymkowitz J (2014) A genome-wide sequence-structure analysis suggests aggregation gatekeepers constitute an evolutionary constrained functional class. J Mol Biol **426:** 2405–2412

De Rybel B, Audenaert D, Vert G, Rozhon W, Mayerhofer J, Peelman F, Coutuer S, Denayer T, Jansen L, Nguyen L, et al (2009) Chemical inhibition of a subset of *Arabidopsis thaliana* GSK3-like kinases activates brassinosteroid signaling. Chem Biol **16:** 594–604

Fernandez-Escamilla A-M, Rousseau F, Schymkowitz J, Serrano L (2004) Prediction of sequence-dependent and mutational effects on the aggregation of peptides and proteins. Nat Biotechnol **22:** 1302–1306

Fitzpatrick AW, Knowles TP, Waudby CA, Vendruscolo M, Dobson CM (2011) Inversion of the balance between hydrophobic and hydrogen bonding interactions in protein folding and aggregation. PLoS Comput Biol **7:** e1002169

Frizzi A, Huang S (2010) Tapping RNA silencing pathways for plant biotechnology. Plant Biotechnol J **8:** 655–677

Ganesan A, Debulpaep M, Wilkinson H, Van Durme J, De Baets G, Jonckheere W, Ramakers M, Ivarsson Y, Zimmermann P, Van Eldere J, Schymkowitz J, Rousseau F (2015) Selectivity of aggregation-determining interactions. J Mol Biol **427:** 236–247

Goldschmidt L, Teng PK, Riek R, Eisenberg D (2010) Identifying the amylome, proteins capable of forming amyloid-like fibrils. Proc Natl Acad Sci USA **107:** 3487–3492

Gudesblat GE, Schneider-Pizoń J, Betti C, Mayerhofer J, Vanhoutte I, van Dongen W, Boeren S, Zhiponova M, de Vries S, Jonak C, Russinova E (2012) SPEECHLESS integrates brassinosteroid and stomata signalling pathways. Nat Cell Biol **14:** 548–554

Hallauer AR, Lamkey KR, White PR (1997) Registration of five inbred lines of maize: B102, B103, B104, B105, and B106. Crop Sci **37:** 1405–1406

Hellemans J, Mortier G, De Paepe A, Speleman F, Vandesompele J (2007) qBase relative quantification framework and software for management and automated analysis of real-time quantitative PCR data. Genome Biol **8:** R19

Irizarry RA, Hobbs B, Collin F, Beazer-Barclay YD, Antonellis KJ, Scherf U, Speed TP (2003) Exploration, normalization, and summaries of high density oligonucleotide array probe level data. Biostatistics **4:** 249–264

Jucker M, Walker LC (2013) Self-propagation of pathogenic protein aggregates in neurodegenerative diseases. Nature **501:** 45–51

Kaganovich D, Kopito R, Frydman J (2008) Misfolded proteins partition between two distinct quality control compartments. Nature **454:** 1088–1095

Karimi M, Bleys A, Vanderhaeghen R, Hilson P (2007) Building blocks for plant gene assembly. Plant Physiol **145:** 1183–1191

Kim T-W, Guan S, Sun Y, Deng Z, Tang W, Shang J-X, Sun Y, Burlingame AL, Wang Z-Y (2009) Brassinosteroid signal transduction from cell-surface receptor kinases to nuclear transcription factors. Nat Cell Biol **11:** 1254–1260

Krebs MR, Morozova-Roche LA, Daniel K, Robinson CV, Dobson CM (2004) Observation of sequence specificity in the seeding of protein amyloid fibrils. Protein Sci **13:** 1933–1938

Li J, Nam KH (2002) Regulation of brassinosteroid signaling by a GSK3/SHAGGY-like kinase. Science **295:** 1299–1301

López De La Paz M, Goldie K, Zurdo J, Lacroix E, Dobson CM, Hoenger A, Serrano L (2002) *De novo* designed peptide-based amyloid fibrils. Proc Natl Acad Sci USA **99:** 16052–16057

Lorberth R, Ritte G, Willmitzer L, Kossmann J (1998) Inhibition of a starch-granule-bound protein leads to modified starch and repression of cold sweetening. Nat Biotechnol **16:** 473–477

Makin OS, Atkins E, Sikorski P, Johansson J, Serpell LC (2005) Molecular basis for amyloid fibril formation and stability. Proc Natl Acad Sci USA **102:** 315–320

Merzlyak EM, Goedhart J, Shcherbo D, Bulina ME, Shcheglov AS, Fradkov AF, Gaintzeva A, Lukyanov KA, Lukyanov S, Gadella TWJ, Chudakov DM (2007) Bright monomeric red fluorescent protein with an extended fluorescence lifetime. Nat Methods **4:** 555–557

Mitraki A (2010) Protein aggregation from inclusion bodies to amyloid and biomaterials. Adv Protein Chem Struct Biol **79:** 89–125

Mitsui T, Itoh K, Hori H, Ito H (2010) Biosynthesis and degradation of starch. Bull Facul Agric Niigata Univ **62:** 49–73

Nelissen H, Rymen B, Jikumaru Y, Demuynck K, Van Lijsebettens M, Kamiya Y, Inzé D, Beemster GTS (2012) A local maximum in gibberellin levels regulates maize leaf growth by spatial control of cell division. Curr Biol **22:** 1183–1187

Nelson R, Sawaya MR, Balbirnie M, Madsen AØ, Riekel C, Grothe R, Eisenberg D (2005) Structure of the cross-β spine of amyloid-like fibrils. Nature **435:** 773–778

Noguchi T, Fujioka S, Choe S, Takatsuto S, Yoshida S, Yuan H, Feldmann KA, Tax FE (1999) Brassinosteroid-insensitive dwarf mutants of Arabidopsis accumulate brassinosteroids. Plant Physiol **121:** 743–752

O'Nuallain B, Williams AD, Westermark P, Wetzel R (2004) Seeding specificity in amyloid growth induced by heterologous fibrils. J Biol Chem **279:** 17490–17499

Payne RW (2012) GenStat Release 15 Reference Manual, Part 3 Procedure Library PL21. VSN International, Hemel Hempstead, UK.

Pillitteri LJ, Sloan DB, Bogenschutz NL, Torii KU (2007) Termination of asymmetric cell division and differentiation of stomata. Nature **445:** 501–505

Price DRG, Gatehouse JA (2008) RNAi-mediated crop protection against insects. Trends Biotechnol **26:** 393–400

Proost S, Van Bel M, Sterck L, Billiau K, Van Parys T, Van de Peer Y, Vandepoele K (2009) PLAZA: a comparative genomics resource to study gene and genome evolution in plants. Plant Cell **21:** 3718–3731

Rajan RS, Illing ME, Bence NF, Kopito RR (2001) Specificity in intracellular protein aggregation and inclusion body formation. Proc Natl Acad Sci USA **98:** 13060–13065

Ren P-H, Lauckner JE, Kachirskaia I, Heuser JE, Melki R, Kopito RR (2009) Cytoplasmic penetration and persistent infection of mammalian cells by polyglutamine aggregates. Nat Cell Biol **11:** 219–225

Richardson JS, Richardson DC (2002) Natural β-sheet proteins use negative design to avoid edge-to-edge aggregation. Proc Natl Acad Sci USA **99:** 2754–2759

Rousseau F, Serrano L, Schymkowitz JWH (2006) How evolutionary pressure against protein aggregation shaped chaperone specificity. J Mol Biol **355:** 1037–1047

Roux M, Schwessinger B, Albrecht C, Chinchilla D, Jones A, Holton N, Malinovsky FG, Tör M, de Vries S, Zipfel C (2011) The *Arabidopsis* leucine-rich repeat receptor-like kinases BAK1/SERK3 and BKK1/SERK4 are required for innate immunity to hemibiotrophic and biotrophic pathogens. Plant Cell **23:** 2440–2455

Rozhon W, Mayerhofer J, Petutschnig E, Fujioka S, Jonak C (2010) ASKθ, a group-III Arabidopsis GSK3, functions in the brassinosteroid signalling pathway. Plant J **62:** 215–223

Sabaté R, Espargaró A, de Groot NS, Valle-Delgado JJ, Fernàndez-Busquets X, Ventura S (2010) The role of protein sequence and amino acid composition in amyloid formation: scrambling and backward reading of IAPP amyloid fibrils. J Mol Biol **404:** 337–352

Sattarzadeh A, Fuller J, Moguel S, Wostrikoff K, Sato S, Covshoff S, Clemente T, Hanson M, Stern DB (2010) Transgenic maize lines with cell-type specific expression of fluorescent proteins in plastids. Plant Biotechnol J **8:** 112–125

Sawaya MR, Sambashivan S, Nelson R, Ivanova MI, Sievers SA, Apostol MI, Thompson MJ, Balbirnie M, Wiltzius JJ, McFarlane HT, et al (2007) Atomic structures of amyloid cross-β spines reveal varied steric zippers. Nature **447:** 453–457

Scacchi E, Osmont KS, Beuchat J, Salinas P, Navarrete-Gómez M, Trigueros M, Ferrándiz C, Hardtke CS (2009) Dynamic, auxin-responsive plasma membrane-to-nucleus movement of *Arabidopsis* BRX. Development **136:** 2059–2067

Sievers F, Wilm A, Dineen D, Gibson TJ, Karplus K, Li W, Lopez R, McWilliam H, Remmert M, Söding J, Thompson JD, Higgins DG (2011) Fast, scalable generation of high-quality protein multiple sequence alignments using Clustal Omega. Mol Syst Biol **7:** 539

Small I (2007) RNAi for revealing and engineering plant gene functions. Curr Opin Biotechnol **18:** 148–153

Storey JD, Tibshirani R (2003) Statistical significance for genomewide studies. Proc Natl Acad Sci USA **100:** 9440–9445

Sugio A, Dreos R, Aparicio F, Maule AJ (2009) The cytosolic protein response as a subcomponent of the wider heat shock response in *Arabidopsis*. Plant Cell **21:** 642–654

Sung DY, Guy CL (2003) Physiological and molecular assessment of altered expression of *Hsc70-1* in Arabidopsis. Evidence for pleiotropic consequences. Plant Physiol **132:** 979–987

Surmacz-Chwedoruk W, Babenko V, Dzwolak W (2014) Master and slave relationship between two types of self-propagating insulin amyloid fibrils. J Phys Chem B **118:** 13582–13589

Szekeres M, Németh K, Koncz-Kálmán Z, Mathur J, Kauschmann A, Altmann T, Rédei GP, Nagy F, Schell J, Koncz C (1996) Brassinosteroids rescue the deficiency of CYP90, a cytochrome P450, controlling cell elongation and de-etiolation in Arabidopsis. Cell **85:** 171–182

Tyedmers J, Mogk A, Bukau B (2010) Cellular strategies for controlling protein aggregation. Nat Rev Mol Cell Biol **11:** 777–788

Van Leene J, Eeckhout D, Cannoot B, De Winne N, Persiau G, Van De Slijke E, Vercruysse L, Dedecker M, Verkest A, Vandepoele K, et al (2015) An improved toolbox to unravel the plant cellular machinery by tandem affinity purification of Arabidopsis protein complexes. Nat Protoc **10:** 169–187

Ventura S, Zurdo J, Narayanan S, Parreño M, Mangues R, Reif B, Chiti F, Giannoni E, Dobson CM, Aviles FX, Serrano L (2004) Short amino acid stretches can mediate amyloid formation in globular proteins: the Src homology 3 (SH3) case. Proc Natl Acad Sci USA **101:** 7258–7263

Vert G, Chory J (2006) Downstream nuclear events in brassinosteroid signalling. Nature **441:** 96–100

Wang ZY, Nakano T, Gendron J, He J, Chen M, Vafeados D, Yang Y, Fujioka S, Yoshida S, Asami T, Chory J (2002) Nuclear-localized BZR1 mediates brassinosteroid-induced growth and feedback suppression of brassinosteroid biosynthesis. Dev Cell **2:** 505–513

Xu J, Reumers J, Couceiro JR, De Smet F, Gallardo R, Rudyak S, Cornelis A, Rozenski J, Zwolinska A, Marine J-C, et al (2011) Gain of function of mutant p53 by coaggregation with multiple tumor suppressors. Nat Chem Biol **7:** 285–295

Yan Z, Zhao J, Peng P, Chihara RK, Li J (2009) BIN2 functions redundantly with other Arabidopsis GSK3-like kinases to regulate brassinosteroid signaling. Plant Physiol **150:** 710–721

Youn JH, Kim TW (2015) Functional insights of plant GSK3-like kinases: multi-taskers in diverse cellular signal transduction pathways. Mol Plant **8:** 552–565

Yu T-S, Kofler H, Häusler RE, Hille D, Flügge U-I, Zeeman SC, Smith AM, Kossmann J, Lloyd J, Ritte G, et al (2001) The Arabidopsis *sex1* mutant is defective in the R1 protein, a general regulator of starch degradation in plants, and not in the chloroplast hexose transporter. Plant Cell **13:** 1907–1918

Zhiponova MK, Vanhoutte I, Boudolf V, Betti C, Dhondt S, Coppens F, Mylle E, Maes S, González-García M-P, Caño-Delgado AI, et al (2013) Brassinosteroid production and signaling differentially control cell division and expansion in the leaf. New Phytol **197:** 490–502

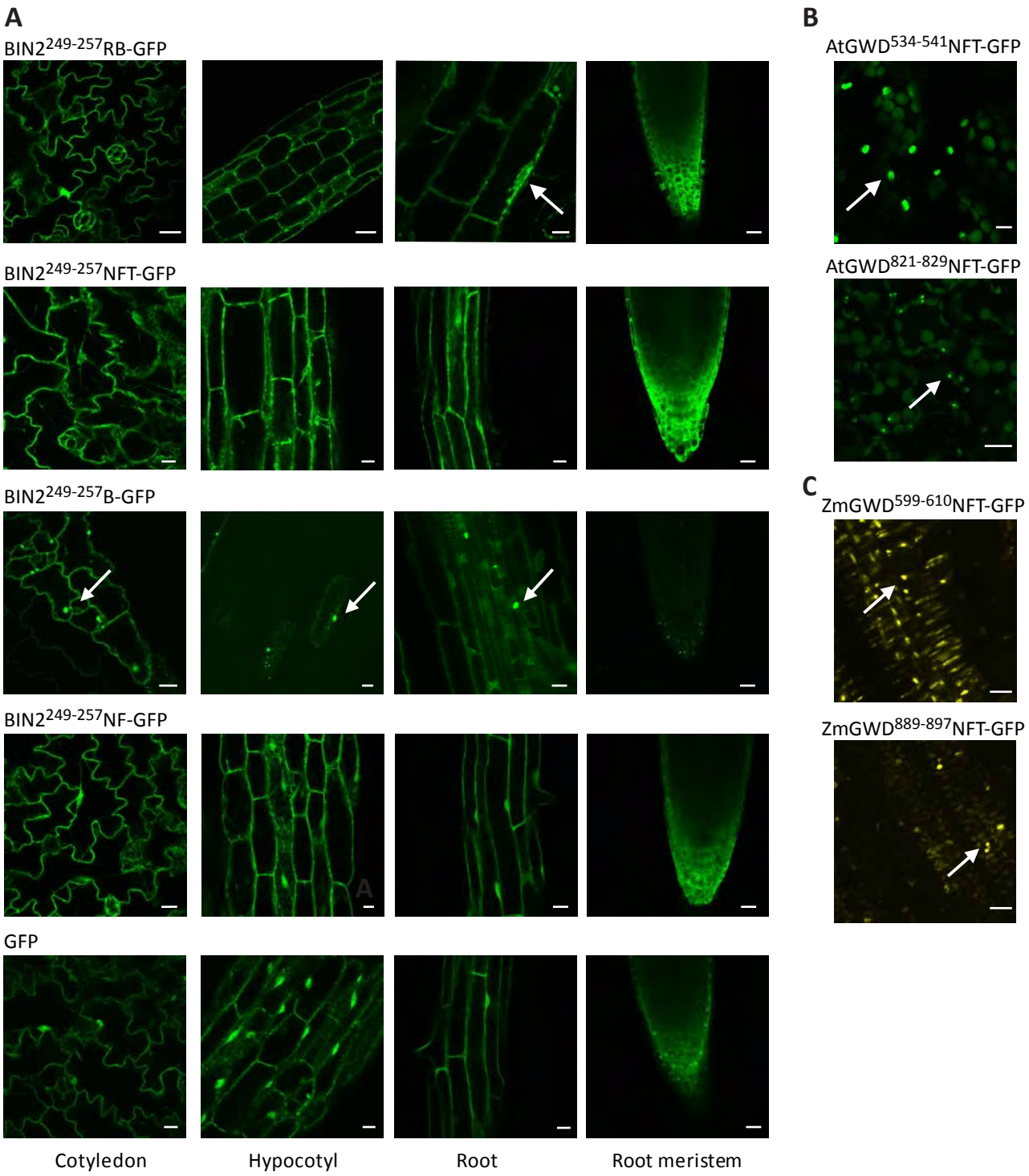

Supplemental Figure S1. Subcellular localization of the aggregates. A, Confocal laser scanning microscope analysis of Arabidopsis 7-day-old T3 transgenic seedlings expressing BIN2$^{249-257}$RB-GFP, BIN2$^{249-257}$NFT-GFP, BIN2$^{249-257}$B-GFP, BIN2$^{249-257}$NF-GFP and free GFP. Different organs are visualized; arrows point to perinuclear aggregates in cells expressing BIN2$^{249-257}$RB-GFP, or to insoluble bodies in BIN2$^{249-257}$B-GFP. Bars, 10 µm. B, Subcellular localization of AtGWD$^{534-541}$NFT-GFP and AtGWD$^{821-829}$NFT-GFP in leaf mesophyll cells of Arabidopsis 7-day-old T3 transgenic seedlings. Arrows point to GFP-labeled chloroplasts. Bars, 10 µm. C, Subcellular localization of ZmGWD$^{599-610}$NFT-YFP, ZmGWD$^{889-897}$NFT-YFP and ZmGWD$^{1082-1088}$NFT-YFP in leaf mesophyll cells of 14-day-old transgenic segregating T1 maize seedlings. Arrows point to YFP-labeled chloroplasts. Scale bars, 20 µm.

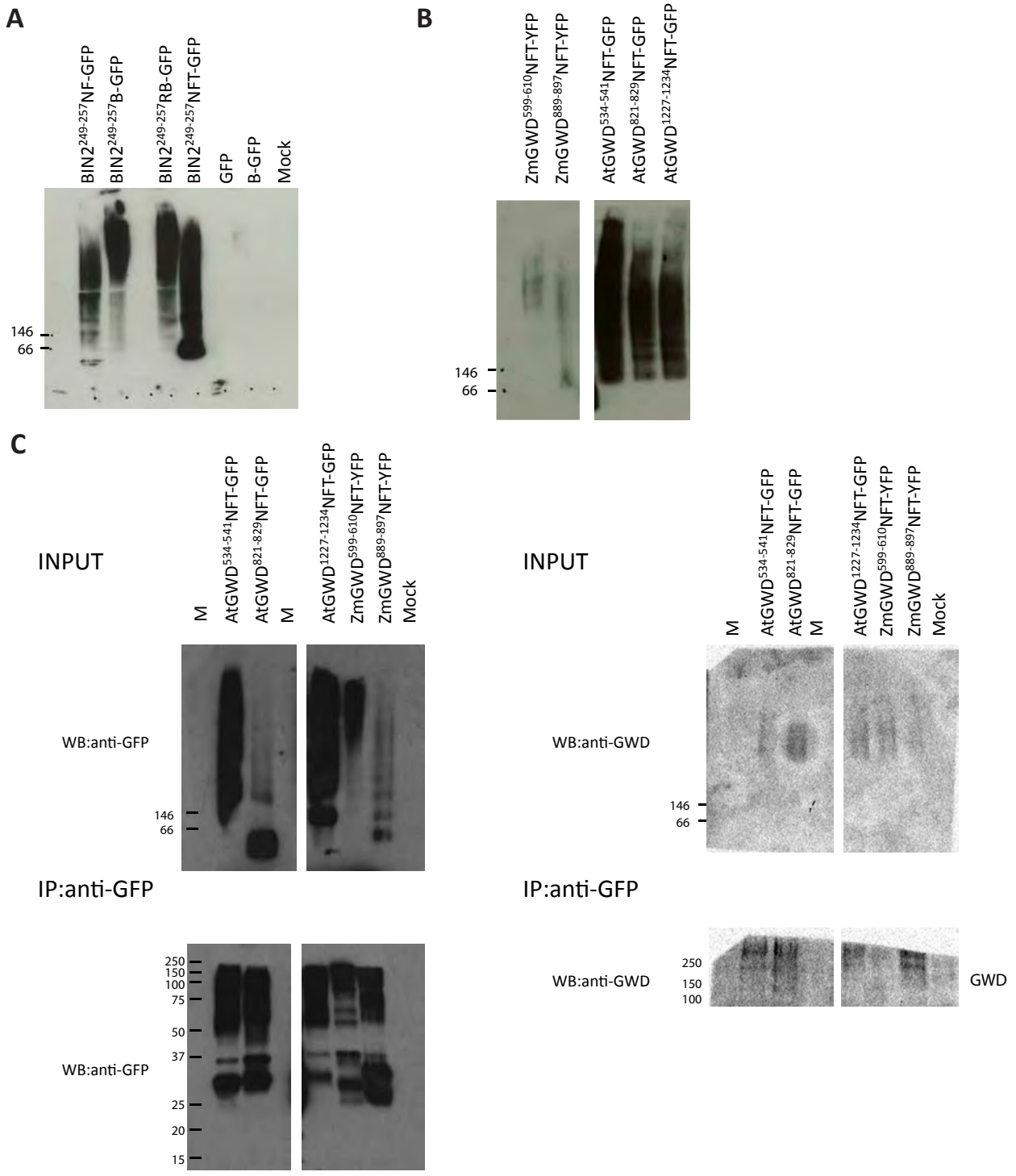

Supplemental Figure S2. Biochemical analysis of the aggregates. A and B, BN-PAGE and immunoblot with anti-GFP antibody on protein aggregates induced in *N. benthamiana* leaves expressing for 3 days different BIN2$^{249-257}$ synthetic aggregating blocks tagged with GFP and compered with wild type (mock), free GFP, and Boost (B)-GFP controls (A) and different GWD APRs tagged with either GFP or YFP (B). C, Co-immunoprecipitation (co-IP) of GWD using anti-GFP antibody-coupled beads from protein extracts derived from tobacco leaves expressing different GWD YFP-tagged APR constructs for 3 days. Left panel: Input (BN-PAGE) and IP developed with anti-GFP antibody; Right panel: Input (BN-PAGE) and IP developed with anti-GWD antibody. The predicted size for GWD is about 156 kDa. BN-PAGE is run in non-denaturing conditions to determine the native masses of protein complexes.

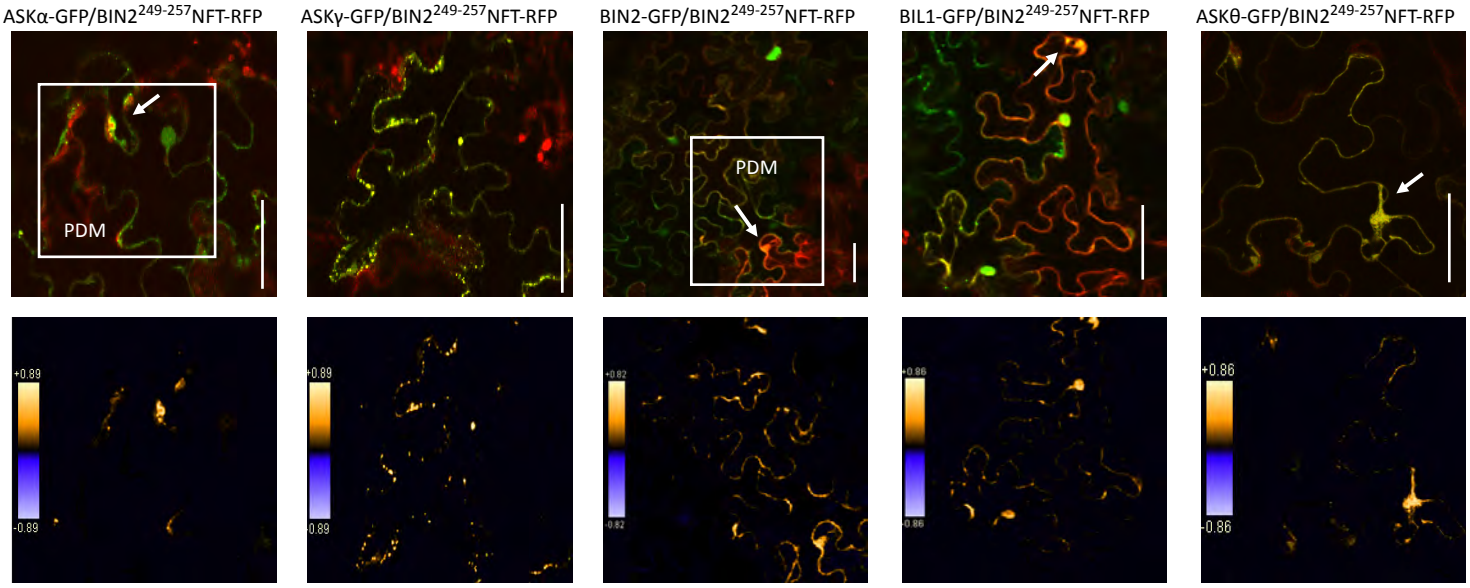

Supplemental Figure S3. Colocalization analysis. Colocalization and corresponding intensity correlation analyses of ASKα-GFP, ASKγ-GFP, ASKθ-GFP, BIN2-GFP, BIL1-GFP coexpressed with BIN2$^{249-257}$NFT-RFP in *N. benthamiana* leaves for 3 days (24 h after BIN2$^{249-257}$NFT-RFP induction with estradiol). Product of the Differences from the Mean (PDM) image at the bottom indicates colocalization quantification for the framed area for which the Mander's coefficient is 0.89 for ASKα and ASKγ, 0.82 for BIN2, and 0.86 for BIL1 and BIL2 (where 0.0 and 1.0 is no and perfect colocalization, respectively). Arrows point to colocalized cytosolic aggregates. Scale bars, 50 µm.

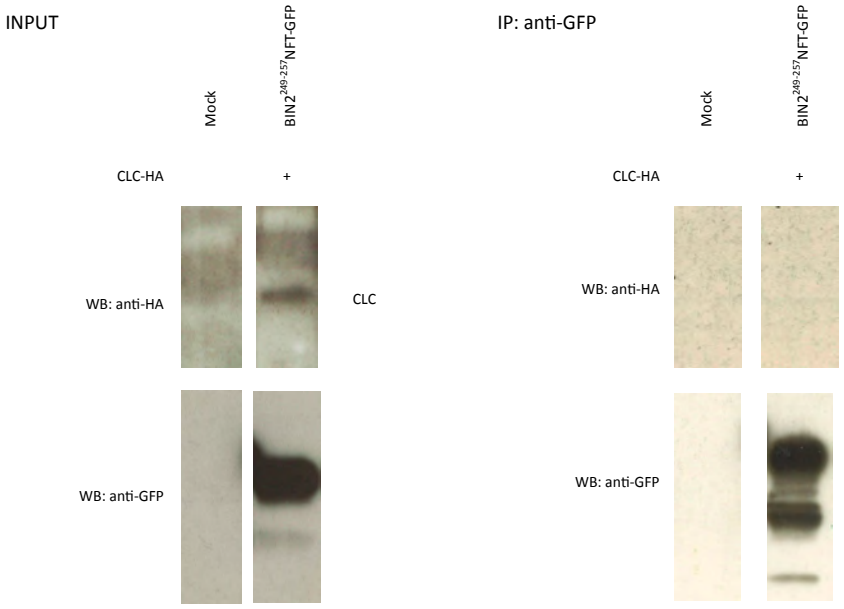

Supplemental Figure S4. Absence of CLC binding by the BIN2 APR. Co-immunoprecipitation (co-IP) of BIN2$^{249\text{-}257}$NFT-GFP with CLC-HA when coproduced for 3 days in *N. benthamiana* leaves. Mock is included as negative control; Protein detection in input and IP immunoblots was done with anti-HA and anti-GFP antibodies, respectively. The predicted size for CLC is about 42 kDa.

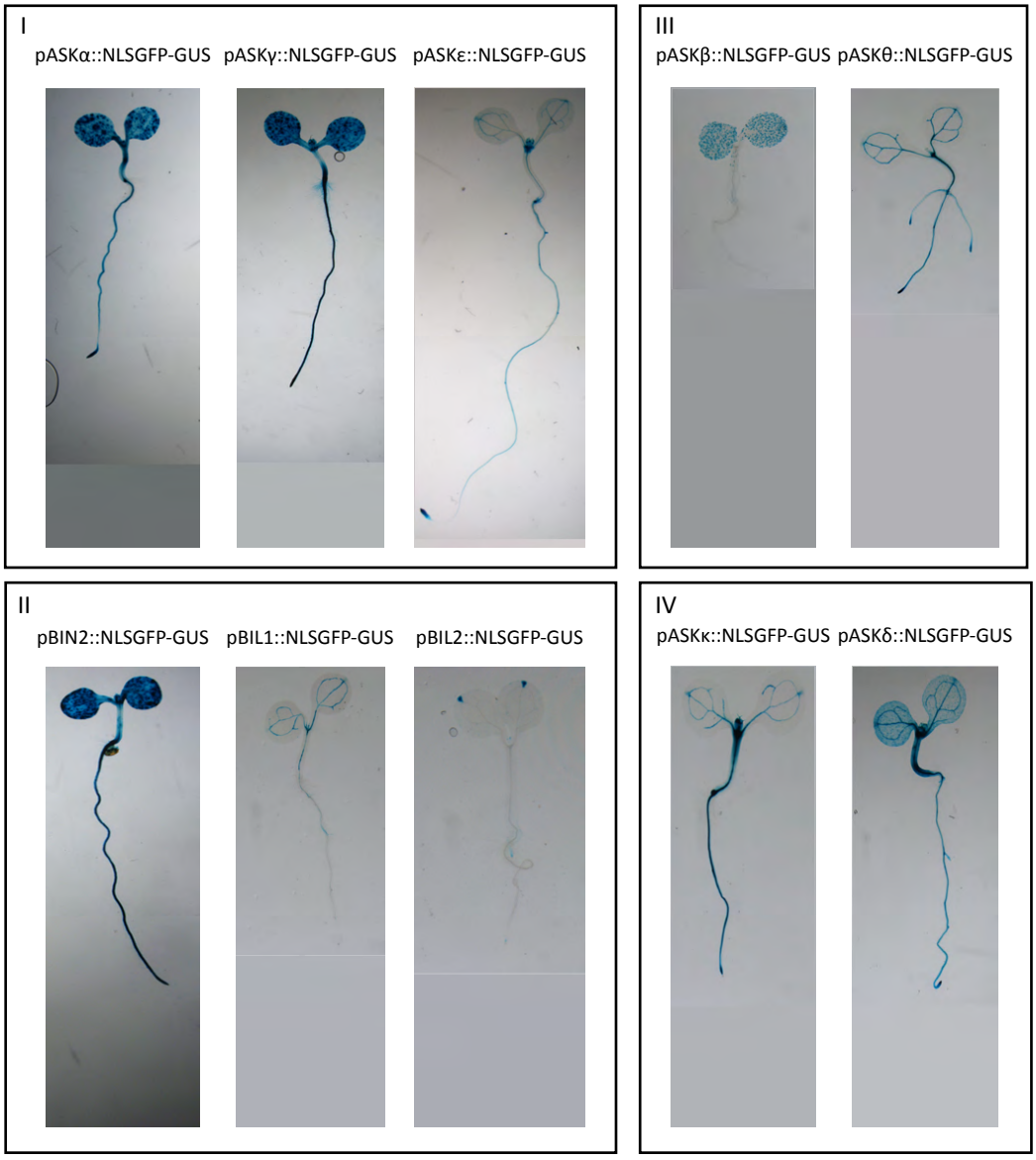

Supplemental Figure S5. ASK promoter-GUS expression patterns. Promoter-GUS analysis of transgenic Arabidopsis plants expressing NLS-GFP-GUS reporters under control of the ASK promoters (pASK). In vitro grown 7-day-old Arabidopsis seedlings were used for histochemical GUS analysis. Stained seedlings expressing different pASK::NLSGFP-GUS constructs are clustered in four groups, according to the ASK family phylogenetic tree, n>6; n, number of seedlings analyzed.

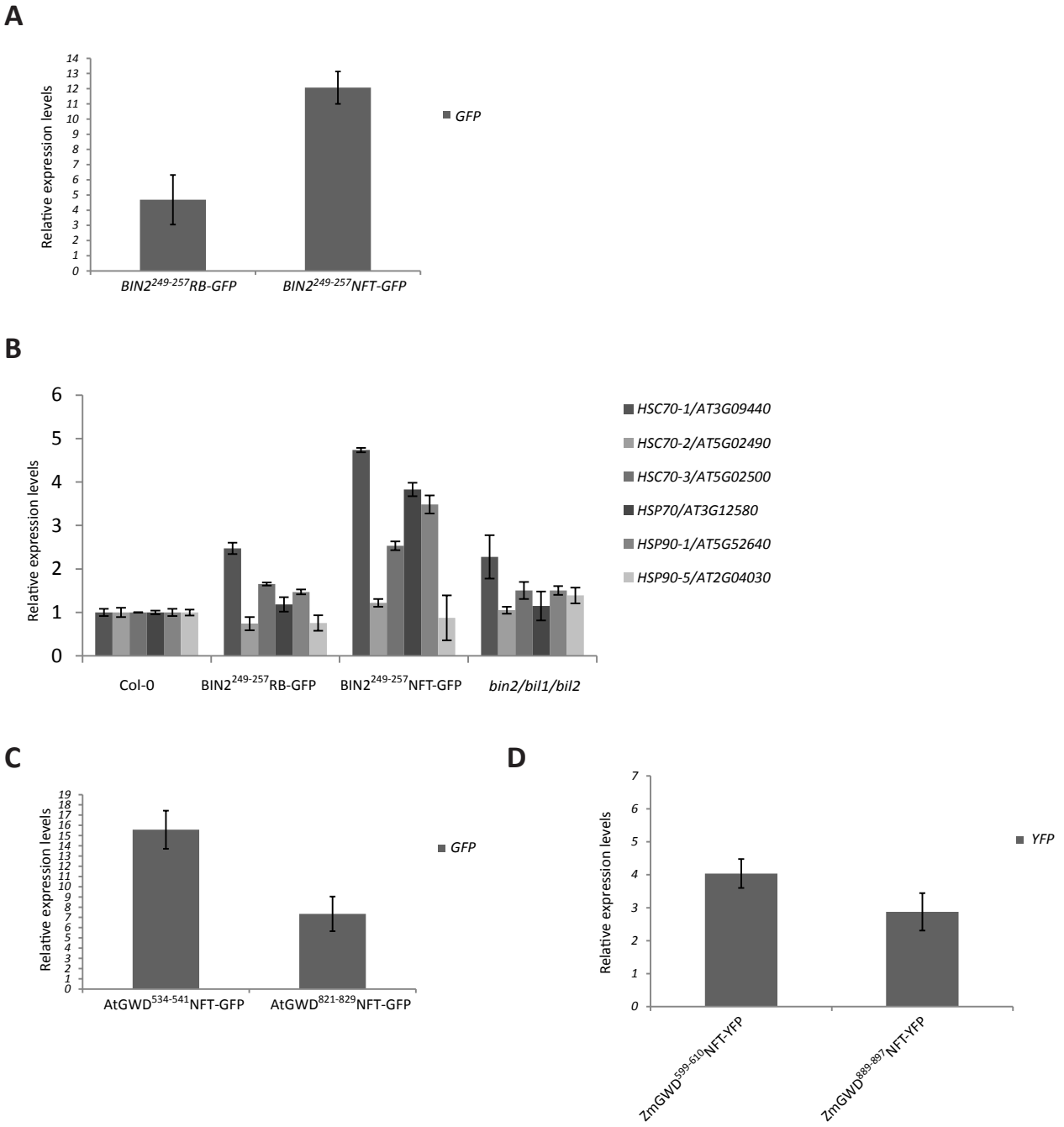

Supplemental Figure S6. Expression analysis of the transgenic lines. A, *GFP* gene expression measured by qRT-PCR in 7-day-old seedlings from homozygous T3 Arabidopsis transgenic lines expressing BIN2$^{249-257}$RB-GFP and BIN2$^{249-257}$NFT-GFP compared to GFP control; reference genotype is the lowest *GFP*-expressing line (from BIN2$^{249-257}$NFT-GFP lines) *CDKA;1* was used as reference gene. B, qRT-PCR analysis of the expression levels of different chaperones (*HSC70-1*, *HSC70-2*, *HSC70-3*, *HSP70*, *HSP90-1* and *HSP90-5*) in 7-day-old Arabidopsis T3 seedlings as in (A). Wild type (Col-0) and *bin2/bil1/bil2* triple mutant were used as controls in three independent experiments and *UBQ10* and *HSF-1* as reference genes. C, *GFP* gene expression measured by qRT-PCR in 7-day-old seedlings from AtGWD$^{534-541}$NFT-GFP and AtGWD8$^{21-829}$NFT-GFP transgenic T3 Arabidopsis lines compared to GFP control; reference genotype is a GFP expressing line; *EF1α* was used as reference gene. D, *YFP* gene expression measured by qRT-PCR in about 30-day-old mature leaves from ZmGWD$^{599-610}$NFT-YFP, ZmGWD$^{889-897}$NFT-YFP and ZmGWD$^{1082-1088}$NFT-YFP transgenic T2 maize lines compared to a reference genotype (the lowest YFP expressing line from ZmGWD$^{889-897}$NFT-YFP lines); *18S* was used as reference gene; n>4; n, for minimum number of T2 plants checked per each maize line. Only expression data for one plant are shown. Error bars indicate SD. Three biological replicas were used for each experiment. All experiments were repeated at least twice with similar results.

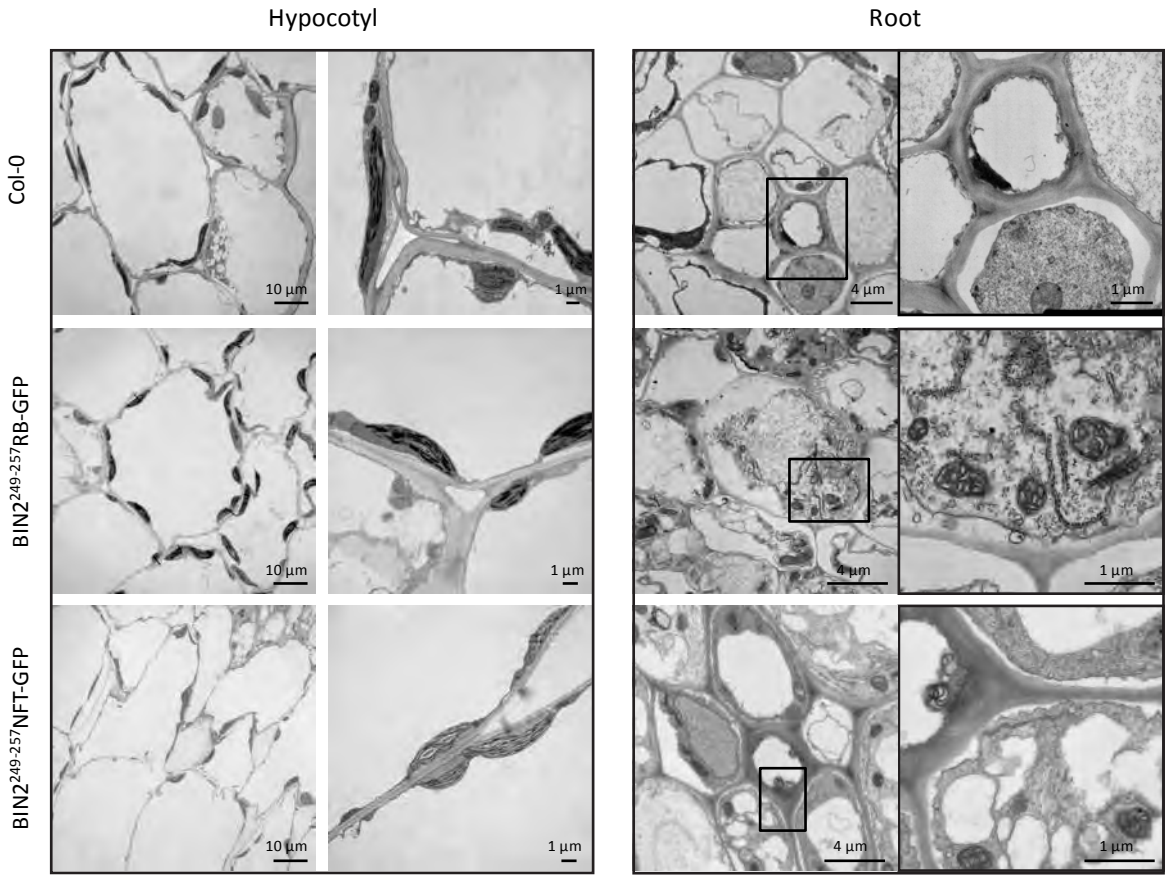

Supplemental Figure S7. TEM analysis. Morphological analysis of BIN2$^{249-257}$APR-expressing plants. TEM micrographs of 7-day-old Arabidopsis seedlings overexpressing BIN2$^{249-257}$RB-GFP and BIN2$^{249-257}$NFT -GFP. Wild type (Col-0) was used as a control. Both hypocotyl and root cells are shown at low and high magnifications. Framed areas are enlarged on the right. Ultra-thin sections were post-stained in uranyl acetate and lead citrate and grids were viewed with a JEM-1010 TEM (Jeol) operating at 80 kV. Scale bars are indicated in each picture.

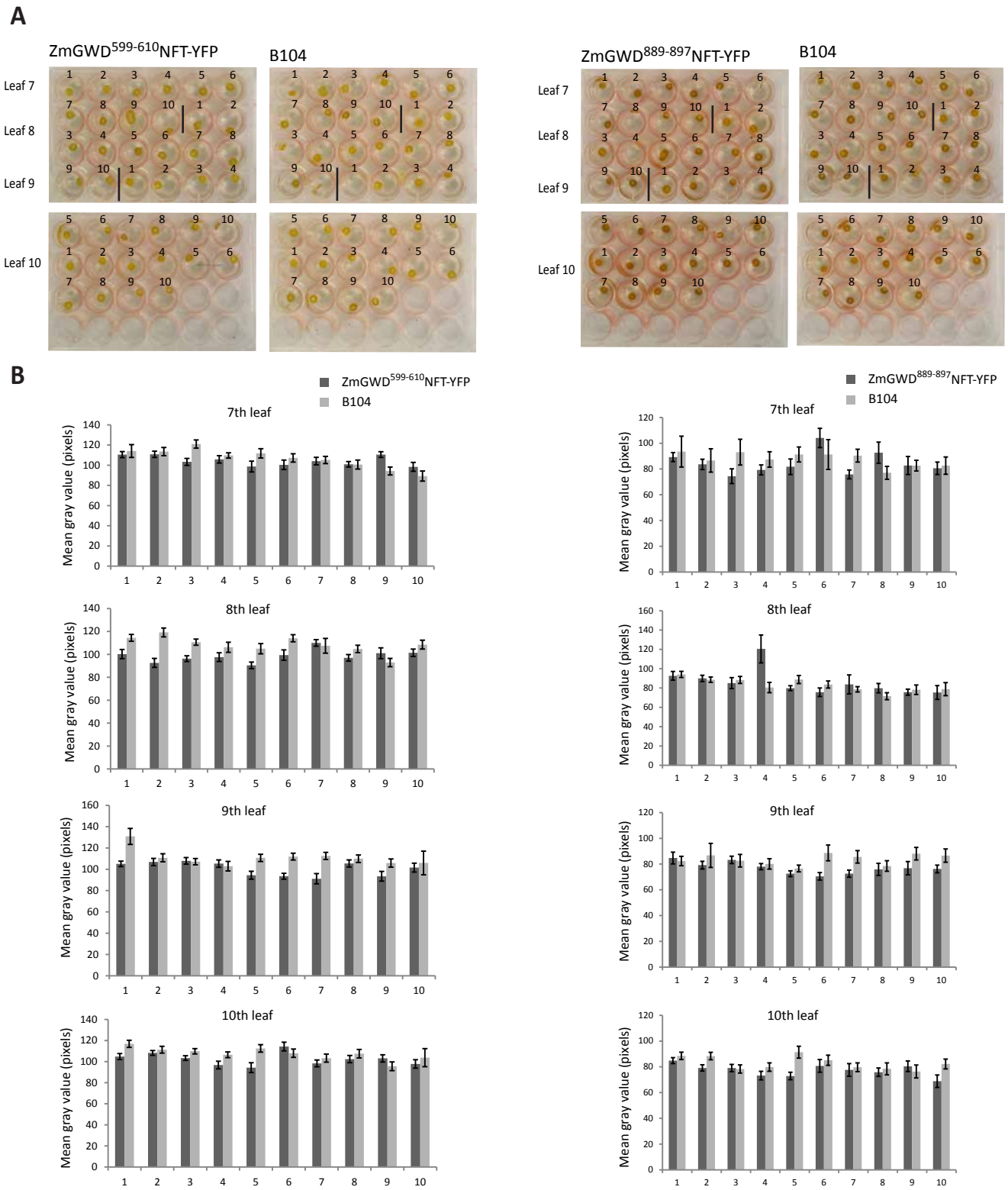

Supplemental Figure S8. Starch content analysis of the transgenic maize lines. A, Lugol staining of 10 punches per mature leaf from the 7th to the 10th leaf of 8-week-old T2-segregating maize lines expressing ZmGWD$^{599-610}$NFT-YFP and ZmGWD$^{889-897}$NFT-YFP shown in Fig. 7. Each leaf punch number and leaf number are indicated. The punches were taken in the mature leaf zone at about 3 cm distance each. B, Quantification of the staining color intensities shown as grey values in pixels, where values from 0 to 250 pixels correspond to color intensities from black to white, respectively.

Fig.3

WB:anti-GFP

Fig.3

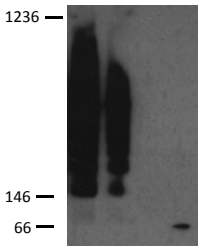

WB:anti-GFP

Fig.S4

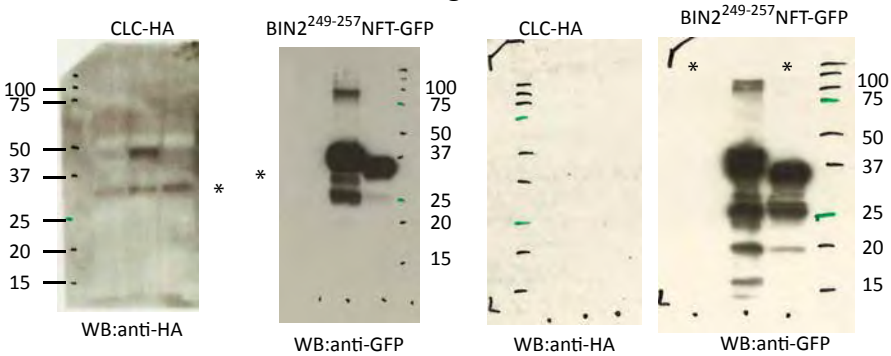

WB:anti-HA | WB:anti-GFP | WB:anti-HA | WB:anti-GFP

Fig.4B

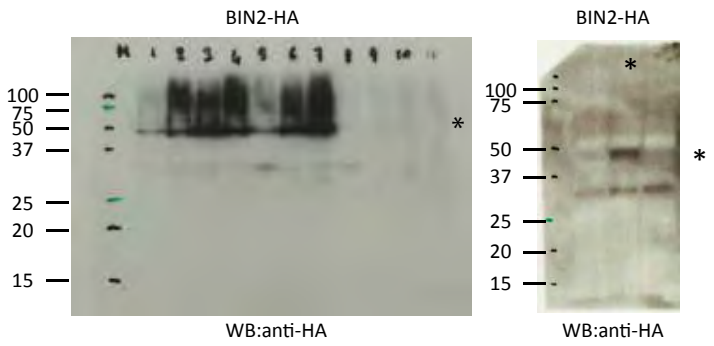

WB:anti-HA | WB:anti-HA

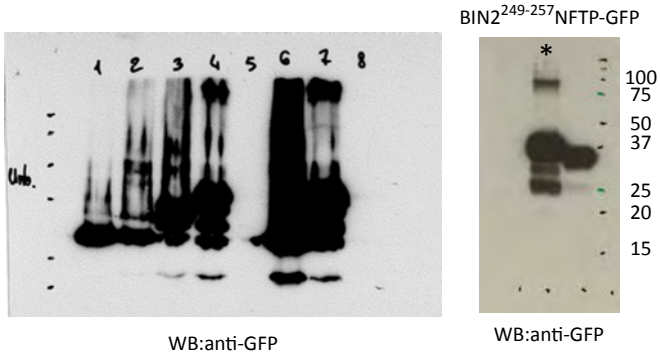

WB:anti-GFP | WB:anti-GFP

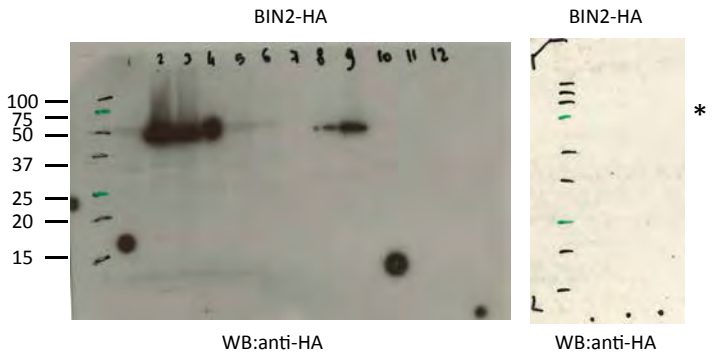

WB:anti-HA | WB:anti-HA

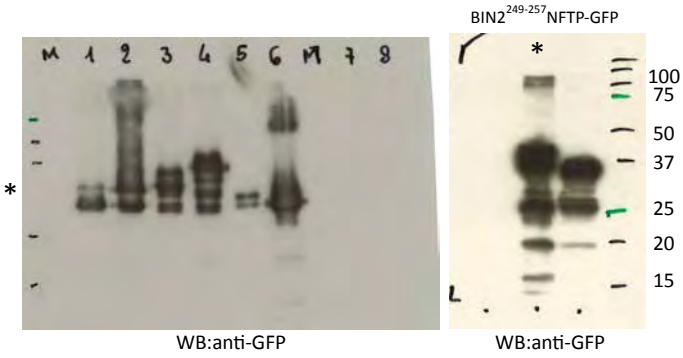

WB:anti-GFP | WB:anti-GFP

Fig.4C

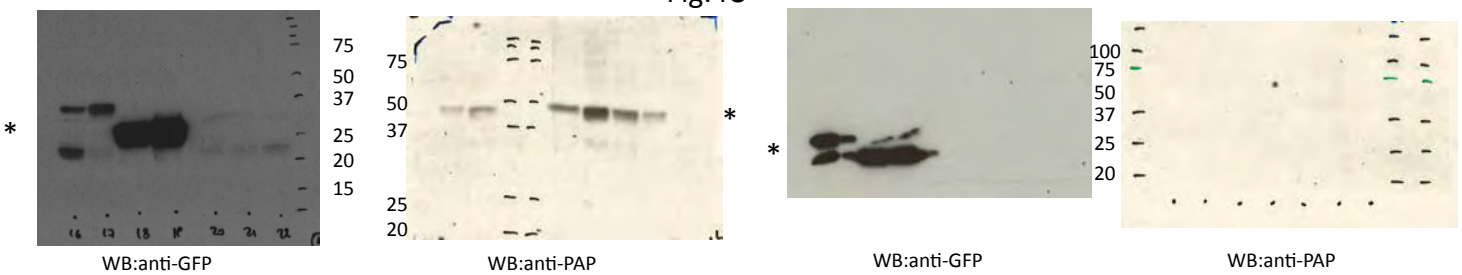

WB:anti-GFP | WB:anti-PAP | WB:anti-GFP | WB:anti-PAP

Fig.S2A,B

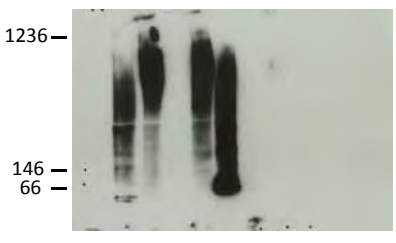

WB:anti-GFP

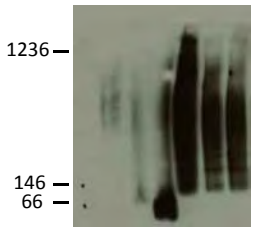

WB:anti-GFP

Fig.S2C

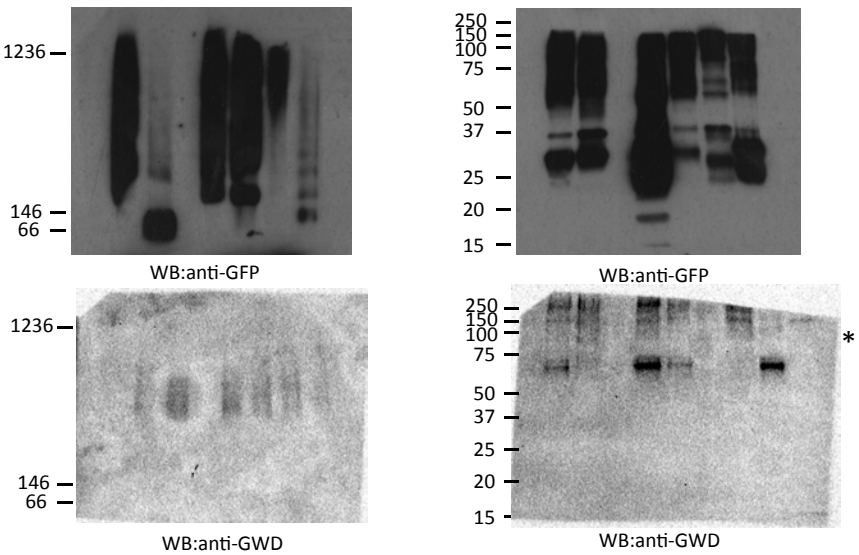

WB:anti-GFP | WB:anti-GFP

WB:anti-GWD | WB:anti-GWD

Supplemental Figure S9. Full scans of immunoblots. Asterisks indicate the bands shown in the figures.

Supplemental Table S4. Protein-protein interactions tested by Bimolecular Fluorescent Complementation (BiFC).

	nGFP-BIN2	**BIN2-cGFP**	**nGFP-BIN2$^{249-257}$NFT**	**BIN2$^{249-257}$NFT-cGFP**	**nGFP**	**cGFP**	**nGFP-MUTE**	**MUTE-nGFP**
nGFP-BIN2	**negative**	not tested	not tested	**positive**	not tested	**negative**	not tested	not tested
BIN2-cGFP	not tested	**negative**	**positive**	not tested	not tested	not tested	not tested	not tested
nGFP-BIN2$^{249-257}$NFT	not tested	**positive**	**negative**	**positive**	not tested	not tested	not tested	not tested
BIN2$^{249-257}$NFT-cGFP	**positive**	not tested	**positive**	**negative**	not tested	not tested	**negative**	**negative**
nGFP-ASKα	not tested	not tested	not tested	**positive**	not tested	**negative**	not tested	not tested
nGFP-ASKγ	not tested	not tested	not tested	**positive**	not tested	**negative**	not tested	not tested
nGFP-ASKε	not tested	not tested	not tested	**positive**	not tested	**negative**	not tested	not tested
nGFP-BIL1	not tested	not tested	not tested	**positive**	not tested	**negative**	not tested	not tested
nGFP-BIL2	not tested	not tested	not tested	**positive**	not tested	**negative**	not tested	not tested
nGFP-ASKθ	not tested	not tested	not tested	**positive**	not tested	**negative**	not tested	not tested
nGFP-ASKβ	not tested	not tested	not tested	**positive**	not tested	**negative**	not tested	not tested
nGFP-ASKδ	not tested	not tested	not tested	**positive**	not tested	**negative**	not tested	not tested
nGFP-ASKκ	not tested	not tested	not tested	**positive**	not tested	**negative**	not tested	not tested
nGFP	not tested	not tested	not tested	not tested	not tested	**negative**	not tested	not tested
cGFP	not tested	not tested	not tested	not tested	**negative**	not tested	**negative**	**negative**
nGFP-MUTE	not tested	not tested	not tested	**negative**	not tested	**negative**	not tested	not tested
MUTE-nGFP	not tested	not tested	not tested	**negative**	not tested	**negative**	not tested	not tested

Supplemental Table S6. Sequence information

A. SABs nucleotide sequences

BIN2$^{249-257}$B	
APR	CAACTTGTTGAAATTATTAAGGTTCTT
Linker	AAACCTGCTGGAGCTGCTAAACCTGGAGCTGCTGGA
Booster	CAGTGGCAGAACTCTACCCTCATCGTTCTCCAGAACTCTACCGTGATTTTC GAACAGAACTCTACCGTTATCTTCGAACAGAAC
BIN2$^{249-257}$RB	
APR	AGACAACTTGTTGAAATTATTAAGGTTCTTAGA
Linker	AAACCTGCTGGAGCTGCTAAACCTGGAGCTGCTGGA
Booster	CAGTGGCAGAACTCTACCCTCATCGTTCTCCAGAACTCTACCGTGATTTTC GAACAGAACTCTACCGTTATCTTCGAACAGAAC
BIN2$^{249-257}$NF	
APR	ATGGCTGATGATAAAGAGGAAAATGCTGTTGATCAATTGGTTGAAATTATT AAAGTTCTTGGAACTCCTACTAGAGAAGAG
Linker	GCTGGTTCTCCTAAAGGAGCTCCTGCTGCTAAAGGATCTGGAGCT
BIN2P$^{249-257}$NFT	
APR	ATGGCTGATGATAAAGAGGAAAATGCTGTTGATCAATTGCCTGAAATTCCT AAAGTTCTTGGAACTCCTACTAGAGAAGAG
Linker	GCTGGTTCTCCTAAAGGAGCTCCTGCTGCTAAAGGATCTGGAGCT
AtGWD$^{534-541}$NFT	
TP	ATGGCTTCTATGATTTCTTCTTCTGCTGTTACTACTGTTTCTAGAGCTTCTA GAGGACAATCTGCTGCTGTTGCTCCTTTTGGAGGACTTAAGTCTATGACT GGATTTCCTGTTAAGAAGGTTAATACTGATATTACTTCTATTACTTCTAATG GAGGAAGAGTTAAGTGT
APR	GAAAATGCTGTTGATTTTGCTGGAATTCTTGTTTGGATGGGAACTCCTACT AGAGAAGAA
Linker	GCTGGATCTCCTAAGGGAGCTCCTGCTGCTAAGGGATCTGGAGCT
AtGWD$^{821-829}$NFT	
TP	ATGGCTTCTATGATTTCTTCTTCTGCTGTTACTACTGTTTCTAGAGCTTCTA GAGGACAATCTGCTGCTGTTGCTCCTTTTGGAGGACTTAAGTCTATGACT GGATTTCCTGTTAAGAAGGTTAATACTGATATTACTTCTATTACTTCTAATG GAGGAAGAGTTAAGTGT
APR	GAAAATGCTGTTGATATTATGTATTTTATTTCTCTTGTTCTTGGAACTCCTA CTAGAGAAGAA
Linker	GCTGGATCTCCTAAGGGAGCTCCTGCTGCTAAGGGATCTGGAGCT
AtGWD$^{1227-1234}$NFT	
TP	ATGGCTTCTATGATTTCTTCTTCTGCTGTTACTACTGTTTCTAGAGCTTCTA GAGGACAATCTGCTGCTGTTGCTCCTTTTGGAGGACTTAAGTCTATGACT GGATTTCCTGTTAAGAAGGTTAATACTGATATTACTTCTATTACTTCTAATG GAGGAAGAGTTAAGTGT
APR	GAAAATGCTGTTGATTATCTTTGTATGGCTGTTCTTGTTACTCCTACTAGA GAAGAA
Linker	GCTGGATCTCCTAAGGGAGCTCCTGCTGCTAAGGGATCTGGAGCT
ZmGWD$^{599-610}$NFT	
TP	ATGGCCAGCATGATCAGCAGCAGCGCCGTGACCACCGTGAGCAGGGCC AGCAGGGGCCAGAGCGCCGCCGTGGCCCCGTTCGGCGGCCTGAAGAGC

	ATGACCGGCTTCCCGGTGAAGAAGGTGAACACCGACATCACCAGCATCA CCAGCAACGGCGGCAGGGTGAAGTGC
APR	GAGAACGCCGTGGACCTGCTGGGCATCGTGGGCCTGTTCGTGTGGATCA GGGGCACCCCGACCAGGGAGGAG
Linker	GCCGGCAGCCCGAAGGGCGCCCCGGCCGCCAAGGGCAGCGGCGCC
ZmGWD$^{889-897}$NFT	
TP	ATGGCCAGCATGATCAGCAGCAGCGCCGTGACCACCGTGAGCAGGGCC AGCAGGGGCCAGAGCGCCGCCGTGGCCCCGTTCGGCGGCCTGAAGAGC ATGACCGGCTTCCCGGTGAAGAAGGTGAACACCGACATCACCAGCATCA CCAGCAACGGCGGCAGGGTGAAGTGC
APR	GAGAACGCCGTGGACATCATGTACTTCATCAGCCTGGTGCTGGGCACCC CGACCAGGGAGGAG
Linker	GCCGGCAGCCCGAAGGGCGCCCCGGCCGCCAAGGGCAGCGGCGCC
ZmGWD$^{1082-1088}$NFT	
TP	ATGGCCAGCATGATCAGCAGCAGCGCCGTGACCACCGTGAGCAGGGCC AGCAGGGGCCAGAGCGCCGCCGTGGCCCCGTTCGGCGGCCTGAAGAGC ATGACCGGCTTCCCGGTGAAGAAGGTGAACACCGACATCACCAGCATCA CCAGCAACGGCGGCAGGGTGAAGTGC
APR	GAGAACGCCGTGGACGTGCTGTTCGCCACCTGCTTCGGCACCCCGACCA GGGAGGAG
Linker	GCCGGCAGCCCGAAGGGCGCCCCGGCCGCCAAGGGCAGCGGCGCC

B. List of primers

Name	**Sequence**	**Purpose**
attB1-APR249R-Boost_F	GGGGACAAGTTTGTACAAAAAAGCAGGCTCCATGAGACAAC TTGTTGAAATTATTAAGGTTCTTAGAAAACCTGCTGGAGCTG CTAA	cloning
attB1-APR249-Boost_F	GGGGACAAGTTTGTACAAAAAAGCAGGCTCCATGCAACTTG TTGAAATTATTAAGGTTCTTAAACCTGCTGGAGCTGCTAA	cloning
APR249R-Boost-attB2_R	GGGGACCACTTTGTACAAGAAAGCTGGGTCTCATCTAAGAA CCTTAATAATTTCAACAAGTTGTCTTCCAGCAGCTCCAGGTT TAG	cloning
APR249-Boost-attB2_R	GGGGACCACTTTGTACAAGAAAGCTGGGTCTCAAAGAACCT TAATAATTTCAACAAGTTGTCCAGCAGCTCCAGGTTTAG	cloning
Boost-attB1_F	GGGGACAAGTTTGTACAAAAAAGCAGGCTCCATGAAACCTG CTGGAGCTGCTAAACC	cloning
Boost-attB2_R	GGGGACCACTTTGTACAAGAAAGCTGGGTCTTACTTGTACA GCTCGTCCATGCC	cloning
ASKγ_prom4-1_FW	GGGGACAACTTTGTATAGAAAAGTTGCTCGTAGCTCAGTTG GTTAGAG	cloning
ASKγ_prom4-1_R	GGGGACTGCTTTTTTGTACAAACTTGCCCCAAGATTAAAACA GAAGA	cloning
ASKθ_prom4-1_FW	GGGGACAACTTTGTATAGAAAAGTTGCTGGGCCTACAACAAT ATCATGT	cloning
ASKθ_prom4-1_R	GGGGACTGCTTTTTTGTACAAACTTGCCTTCGCTTTATTCAC CAACC	cloning
ASKε_prom4-1_FW	GGGGACAACTTTGTATAGAAAAGTTGCTCTGTTTATTGTTATA GAGAG	cloning
ASKε_prom4-1_R	GGGGACTGCTTTTTTGTACAAACTTGCATGTATTCAAGATCT TTAATT	cloning
ASKα_prom4-1_FW	GGGGACAACTTTGTATAGAAAAGTTGCTGACATGTTTTCGTC TAAGATT	cloning

ASKα_prom4-1_R	GGGGACTGCTTTTTTGTACAAACTTGCTTTTCAGGCTACAAAACTCT	cloning
ASKβ_prom4-1_F	GGGGACAACTTTGTATAGAAAAGTTGCTAACAAAGAATGTTGTAATTT	cloning
ASKβ_prom4-1_R	GGGGACTGCTTTTTTGTACAAACTTGCCGTTTTTTTCTTCTTAAAAAAGC	cloning
ASKδ_prom4-1_F	GGGGACAACTTTGTATAGAAAAGTTGCTCATGAGCCATAACCGAGAAA	cloning
ASKδ_prom4-1_R	GGGGACTGCTTTTTTGTACAAACTTGCGGTGGTGGTTGTTCGGAAGA	cloning
BIL1_prom4-1_F	GGGGACAACTTTGTATAGAAAAGTTGCTATATCATGTTAAAAGAAAATTTC	cloning
BIL1_prom4-1_R	GGGGACTGCTTTTTTGTACAAACTTGCGTGCTTTTACAGCTCTAACT	cloning
BIN2_prom4-1_2_F	GGGGACAACTTTGTATAGAAAAGTTGCTCATTTCTTTTTGCCGACGGTTG	cloning
BIN2_prom4-1_2_R	GGGGACTGCTTTTTTGTACAAACTTGCGGCGATAGAGACACAGAGAGGAG	cloning
BIL2_prom4-1_F	GGGGACAACTTTGTATAGAAAAGTTGCTATTTTACTGGTATCTTCTTT	cloning
BIL2_prom4-1_R	GGGGACTGCTTTTTTGTACAAACTTGCGTGCTTTTTTACTCTTTTCT	cloning
ASKκ_prom4-1_F	GGGGACAACTTTGTATAGAAAAGTTGCTTAAGTACGTTCATTATCATG	cloning
ASKκ_prom4-1_R	GGGGACTGCTTTTTTGTACAAACTTGCGATATATATTCAGAAGATAAC	cloning
attB1F_ASKα_CDS	GGGGACAAGTTTGTACAAAAAAGCAGGCTCAATGGCGTCAGTGGGTATAGC	cloning
attB2R_ASKα_CDS	GGGGACCACTTTGTACAAGAAAGCTGGGTACAAACCGAGCCAAGGACACT	cloning
attB1F_ASKγ_CDS	GGGGACAAGTTTGTACAAAAAAGCAGGCTCAATGGCCTCGGTGGGCATAGA	cloning
attB2R_ASKγ_CDS	GGGGACCACTTTGTACAAGAAAGCTGGGTACAAACTGAGCCACGGACATTG	cloning
attB1F_ASKε_CDS	GGGGACAAGTTTGTACAAAAAAGCAGGCTCAATGGCTTCTGTGGGAACATT	cloning
attB2R_ASKε_CDS	GGGGACCACTTTGTACAAGAAAGCTGGGTAGAGAGCGAGGAAGGAACATT	cloning
attB1F_BIL2_CDS	GGGGACAAGTTTGTACAAAAAAGCAGGCTCAATGGCCTCATTACCATTGGGGCCTCAGCCTCATGCT	cloning
attB2R_BIL2_CDS	GGGGACCACTTTGTACAAGAAAGCTGGGTAACTGTTTTGTAATCCTGTGCTCATTTGTCGTCTC	cloning
attB1F_BIL1_CDS	GGGGACAAGTTTGTACAAAAAAGCAGGCTCAATGACTTCGATACCATTGGG	cloning
attB2R_BIL1_CDS	GGGGACCACTTTGTACAAGAAAGCTGGGTAGGGTCCAGCTTGAAATGGAA	cloning
attB1F_ASKθ_CDS	GGGGACAAGTTTGTACAAAAAAGCAGGCTCAATGAACGTGATGCGTCGTCT	cloning
attB2R_ASKθ_CDS	GGGGACCACTTTGTACAAGAAAGCTGGGTAAGAGCTACTTCCCGTTCCCT	cloning
attB1F_BIN2_CDS	GGGGACAAGTTTGTACAAAAAAGCAGGCTCAATGGCTGATGATAAGGAGAT	cloning
attB2R_BIN2_CDS	GGGGACCACTTTGTACAAGAAAGCTGGGTAAGTTCCAGATTGATTCAAGA	cloning
attB2R_BIN2_CDS_stop	GGGGACCACTTTGTACAAGAAAGCTGGGTATTAAGTTCCAGATTGATTCAAGA	cloning
attB1F_ASKβ_CDS	GGGGACAAGTTTGTACAAAAAAGCAGGCTCAATGAATGTGGTGCGGAGATT	cloning

attB2R_ASKβ_CDS	GGGGACCACTTTGTACAAGAAAGCTGGGTATTTCCTTGCATGCTCAG	cloning
attB1F_ASKκ_CDS	GGGGACAAGTTTGTACAAAAAAGCAGGCTCAATGGCATCCTCTGGACTGGG	cloning
attB2R_ASKκ_CDS	GGGGACCACTTTGTACAAGAAAGCTGGGTACGAATGCAAAGCCATGA	cloning
attB1F_ASKδ_CDS	GGGGACAAGTTTGTACAAAAAAGCAGGCTCAATGGAATCTCATCTGGGAAA	cloning
attB2R_ASKδ_CDS	GGGGACCACTTTGTACAAGAAAGCTGGGTACGAGTGTAATGCCATGA	cloning
ASKα_stop_attb1F	GGGGACAAGTTTGTACAAAAAAGCAGGCTCAATGGCGTCAGTGGGTATAGC	cloning
ASKα_stop_attb2R	GGGGACCACTTTGTACAAGAAAGCTGGGTCTCACAAACCGAGCCAAGGAC	cloning
ASKγ_stop_attb1F	GGGGACAAGTTTGTACAAAAAAGCAGGCTCAATGGCCTCGGTGGGCATAGA	cloning
ASKγ_stop_attb2R	GGGGACCACTTTGTACAAGAAAGCTGGGTCTCACAAACTGAGCCACGGAC	cloning
ASKε_stop_attb1F	GGGGACAAGTTTGTACAAAAAAGCAGGCTCAATGGCTTCTGTGGGAACATT	cloning
ASKε_stop_attb2R	GGGGACCACTTTGTACAAGAAAGCTGGGTCTTAGAGAGCGAGGAAGGAAC	cloning
BIL1_stop_attb1F	GGGGACAAGTTTGTACAAAAAAGCAGGCTCAATGACTTCGATACCATTGGG	cloning
BIL1_stop_attb2R	GGGGACCACTTTGTACAAGAAAGCTGGGTCCTAGGGTCCAGCTTGAAATG	cloning
BIL2_stop_attb1F	GGGGACAAGTTTGTACAAAAAAGCAGGCTCAATGGCCTCATTACCATTGGG	cloning
BIL2_stop_attb2R	GGGGACCACTTTGTACAAGAAAGCTGGGTCTTAACTGTTTTGTAATCCTG	cloning
ASKθ_stop_attb1F	GGGGACAAGTTTGTACAAAAAAGCAGGCTCAATGAACGTGATGCGTCGTCT	cloning
ASKθ_stop_attb2R	GGGGACCACTTTGTACAAGAAAGCTGGGTCCTAAGAGCTACTTCCCGTTC	cloning
p35S_F	CCACTATCCTTCGCAAGACCC	sequencing
GFP_R	GTTTACGTCGCCGTCCAGCT	sequencing
bri1_F	TCAAGCTTCACCATCTCAGTCT	genotyping
bri1_R	GCACCGGAGATTGAATTCGC	genotyping
DWF4_F	GTGATCTCAGCCGTACATTTGGA	qPCR
DWF4_R	CACGTCGAAAAACTACCACTTCCT	qPCR
CPD_F	GAATGGAGTGATTACAAGTC	qPCR
CPD_R	GTGAACACATTAGAAGGGCCTG	qPCR
BZR1_F	CCTCTACATTCTTCCCTTTCCTCAG	qPCR
BZR1_R	GCTTAGCGATAGATTCCCAGTTAGG	qPCR
GFP_F	GAAGCGCGATCACATGGT	qPCR
GFP_R	CCATGCCGAGAGTGATCC	qPCR
ZmYFP_F	GAGCTGAAGGGCATCGACTT	qPCR
ZmYFP_R	TTCTGCTTGTCGGCCATGAT	qPCR
CDKA;1_F	ATGGCGTGGGGTAACTTCTCTA	qPCR
CDKA;1_R	TTGGTCGGATCCATTAACAGCA	qPCR
Zm18S_F	ACCTTACCAGCCCTTGACATATG	qPCR
Zm18S_R	GACTTGACCAAACATCTCACGAC	qPCR
EF1A_F	CTGGAGGTTTTGAGGCTGGTAT	qPCR

EF1AF_R	CCAAGGCTGAAAGCAAGAAGA	qPCR
AT-HSC70-1/AT3G09440_F	GCT ATT CTC AGC GGT GAA GG	qPCR
AT-HSC70-1/AT3G09440_R	TTC TCG TCT TGG ATG GTG TTC	qPCR
AT-HSC70-1/AT3G09440_Probe	/56-FAM/TC TTC GGA C/Zen/T TGT ACT TCT CAG CCT CT/3IABkFQ/	qPCR
AT-HSC70-2/AT5G02490_F	GAA ACA GAA CCA CTC CCT CG	qPCR
AT-HSC70-2/AT5G02490_R	CCA ATC AAC CTC TTT GCA TCG	qPCR
AT-HSC70-2/AT5G02490_Probe	/56-FAM/AG AAC CAA G/Zen/T CGC CAT GAA CCC T/3IABkFQ/	qPCR
AT-HSC70-3/AT5G02500_F	AAC AGA ACC ACA CCG TCT TAC	qPCR
AT-HSC70-3/AT5G02500_R	ACC AAT CAA CCT CTT CGC ATC	qPCR
AT-HSC70-3/AT5G02500_Probe	/56-FAM/CG TCA CCA A/Zen/T CAA CCG TTC GCT ATC A/3IABkFQ/	qPCR
AT-HSP70/AT3G12580_F	TGA CTC TTA TCC GCT TGA ACA G	qPCR
AT-HSP70/AT3G12580_R	TCC TAC GTT GCT TTC ACT GAC	qPCR
AT-HSP70/AT3G12580_Probe	/56-FAM/TC GCC ATG A/Zen/A CCC TAC CAA CAC C/3IABkFQ/	qPCR
AT-HSP90-1/AT5G52640_F	GTG GTT CCT TCA CTG TCA CTA G	qPCR
AT-HSP90-1/AT5G52640_R	TTC ACC AAG TCT TTG AGT CTC C	qPCR
AT-HSP90-1/AT5G52640_Probe	/56-FAM/TC CTC CAA G/Zen/T ATT CAA GCT GAT CGT CCT /3IABkFQ/	qPCR
AT-HSP90-5/AT2G04030_F	GAA CTC AAC CTC ACC CTC AG	qPCR
AT-HSP90-5/AT2G04030_R	ACT AGC CAA CGA GAC CAA AC	qPCR
AT-HSP90-5/AT2G04030_Probe	/56-FAM/TC CAC TTG C/Zen/T CAC ACA CAC TTC ACA /3IABkFQ/	qPCR
AT-UBQ10/AT4G05320 _F	CTC CTT ATC CTG GAT CTT GGC	qPCR
AT-UBQ10/AT4G05320 _R	TTT CTC TCA ATT CTC TCT ACC GTG	qPCR
AT-UBQ10/AT4G05320 _Probe	/56-FAM/TC GAG GGT G/Zen/A TTG TCT TTC CGG TG/3IABkFQ/	qPCR
AT-HSF1/AT4G17750_F	CCT TCA TTA GCA AAT TCC CAT CG	qPCR

AT-HSF1/AT4G17750_R	TCA TTG TTT GGG ATC CAC CG	qPCR
AT-HSF1/AT4G17750_Probe	/56-FAM/CA ATT TCT C/Zen/C AGC TTT GTT CGC CAG T/3IABkFQ/	qPCR
pPEPC_end	GGTTCCGTTGCGGTTA	genotyping
pT35S.1	ACCCTAATTCCCTTATCTGG	genotyping